THE UNIVERSITY OF ALBERTA

MAGNETIC STABILIZATION OF PULSED LASERS

by

WALTER D. BILIDA

A THESIS

SUBMITTED TO THE FACULTY OF GRADUATE STUDIES AND RESEARCH

IN PARTIAL FULFILMENT OF THE REQUIREMENTS FOR THE DEGREE

OF MASTER OF SCIENCE

DEPARTMENT OF ELECTRICAL ENGINEERING

EDMONTON, ALBERTA

FALL 1989

THE UNIVERSITY OF ALBERTA

RELEASE FORM

NAME OF AUTHOR WALTER D. BILIDA

TITLE OF THESIS MAGNETIC STABILIZATION OF PULSED LASERS

DEGREE FOR WHICH THESIS WAS PRESENTED MASTER OF SCIENCE

YEAR THIS DEGREE GRANTED FALL 1989

Permission is hereby granted to THE UNIVERSITY OF ALBERTA LIBRARY to reproduce single copies of this thesis and to lend or sell such copies for private, scholarly or scientific research purposes only.

The author reserves other publication rights, and neither the thesis nor extensive extracts from it may be printed or otherwise reproduced without the author's written permission.

(SIGNED) Walter Bilida

PERMANENT ADDRESS:

[illegible]

[illegible]

[illegible]

DATED 21 MAY 1989

THE UNIVERSITY OF ALBERTA

FACULTY OF GRADUATE STUDIES AND RESEARCH

The undersigned certify that they have read, and recommend to the Faculty of Graduate Studies and Research, for acceptance, a thesis entitled MAGNETIC STABILIZATION OF PULSED LASERS submitted by WALTER D. BILIDA in partial fulfilment of the requirements for the degree of MASTER OF SCIENCE.

Supervisor

Supervisor

External Examiner

Date 26 MAY 89

Dedication

To my father, for his never ending encouragement and support.

Abstract

Avalanche discharge pumped excimer lasers provide a convenient source of high power ultraviolet radiation. The application of this newly developed laser system has been exploited in several areas, of which microelectronic etching and laser surgery are among the newest. In typical UV preionized excimer laser systems, laser pulses are less than 50 nanoseconds in duration. However if longer optical pulses could be obtained from these lasers, important operational features such as narrowing of the spectral width, mode locking, improvement of spatial quality, and reduced peak power levels would become possible. Such operational characteristics are highly desirable in a wide range of applications including medical, scientific and industrial.

Conventional methods used to increase this optical pulse length have largely failed, since the laser output was found to prematurely terminate while the laser was under strong electrical excitation. The cause of this early termination was linked to the collapse of an initially uniformly excited gain media, into narrow filamentary channels. The object of this thesis, is therefore to investigate an alternative pulse stretching approach based on the magnetic stabilization concept, which will be used to postpone the formation of these filamentary channels for the entire discharge duration; thereby providing long pulse operation of these excimer devices.

The process of using magnetic fields to stabilize gas discharges has been previously demonstrated in low pressure, continuous wave laser systems. The technique in effect provides stabilization by suppressing the formation of thermal instabilities, through the application of magnetic fields transverse to the electric field direction. As a consequence, charge carriers are deflected in a direction orthogonal to both the electric and magnetic field vectors, thereby sweeping an incipiently unstable electron avalanche into regions having smaller instability growth rates.

The initial purpose of this thesis was to apply the magnetic stabilization concept to pulsed discharges operating at, or near, atmospheric pressure. In the adaptation of the process, a pulsed electromagnet was designed, which produced radially profiled magnetic fields

in the 0.4 T range. In conjunction with this magnet, three different discharge geometries were built and tested. It was found that a cylindrical structure, with separate control over both the magnetic and electric fields, proved to be the most effective. Thus, a pulsed electromagnet, interfaced with a low inductance cylindrical discharge geometry was developed to apply the magnetic stabilization concept to TEA discharges.

Theoretical analysis, featuring charge carrier motion, was done to further understand the processes involved under pulsed excitation. This analysis revealed that under the short excitation times necessary for stable discharge operation, charge carrier drifts are greatly reduced, in comparison to a low pressure laser system. The theoretical results projected that to achieve a magnetically stabilized pulsed discharge, magnetic field strengths of $\simeq$ 2.4 T are required. With this field strength, transverse electron drift distances of about 1 mm can be achieved. This aspect satisfies the condition of deflecting electron avalanches into lower growth areas.

Using a previously designed test vessel, experimental data revealed transverse electron drifts of only 0.3 mm. Consequently, the magnetic stabilization technique was not effective in the suppression of thermal instabilities. Because of the inherent limitation with the electromagnet structure available in the laboratory, the 2.4 T field necessary for the effect to become observable could not be produced. The attainment of much stronger magnetic fields, possibly through the use of a new generation of extremely strong Samarium permanent magnets, developed by Sherritt Gordon Ltd., should conceivably confirm the viability of the approach.

Acknowledgements

The author would like to thank his supervisors, Dr. C.E. Capjack and Dr. H.J.J. Seguin, for their continual support and guidance.

Additional thanks goes to various members of the laboratory for their specialized assistance. Specifically to Dr. S.K. Nikumb for his experimental help and scientific advice, as well as to Mr. H. Reshef for his mechanical expertice. Electronic assistance was provided by Mr. D. Presakarchuk and Mr. D. Akitt. In addition, most of the figures included in this thesis were produced by Mr. V. Pohnert. Further thanks goes out to Mr. A. Labun and Mr. U. Yelden for their general constructive criticism.

Table of Contents

Chapter		Page
1.	INTRODUCTION	1
	1.1 The Magnetic Stabilization Concept	2
	1.2 Motivation	3
	1.3 Historical Development of Pulsed Lasers	4
	1.3.1 Three and Four Level Lasers	4
	1.3.2 Solid State Lasers	6
	1.3.3 The CO_2 Laser	7
	1.3.4 The Excimer Laser	7
	1.4 Methods of Excitation	7
	1.4.1 Optical Pumping	8
	1.4.2 Pumping with Self-Sustained Electric Discharges	8
	1.4.3 Ionizational Pumping	12
	1.4.3.1 E-Beam Sustained Excitation	12
	1.4.4 Thermal Pumping	14
	1.5 Gas Kinetics of The CO_2 Laser	15
	1.5.1 Vibrational Modes in CO_2 and N_2	15
	1.5.2 Excitation and Relaxation of the CO_2 Laser	15
	1.6 Gas Kinetics of The KrF Laser	18
	1.6.1 Electron Beam Pumped Excimer Systems	18
	1.6.2 Avalanche Discharge Pumped Systems	21
	1.6.3 Laser Emission and Relaxation of the KrF Laser	22
2.	SYSTEM DESIGN	25
	2.1 Pulsed Electromagnet	26
	2.2 TEA Discharge Geometry	28
	2.3 Modified TEA Discharge System	31

2.4 Rail Gun TEA System 34

3. THEORETICAL ANALYSIS 40

3.1 Momentum Transfer Collisional Frequency 40

3.2 Cyclotron Frequency 44

3.3 Hall Parameter 44

3.4 Drift Calculation 45

3.5 Instability Mechanisms 50

3.6 Thermal Instability Formation Time 51

4. RESULTS 57

4.1 Experimental Discharge Data 57

5. CONCLUSIONS 63

List of Tables

Table		Page
3.1	Fundamental Discharge Parameters.	41
3.2	Momentum Transfer Cross Sections.[18,19]	41
3.3	Electron - Ion E x B, and E-Field Drift Velocities.	47
3.4	Variables used in Equation 3.19.[22]	54
4.1	Data on a 12/14/74 Mixture with a 300 ns Excitation Length	59
4.2	Data on a 12/14/74 Mixture with a 800 ns Excitation Length	59
4.3	Data on a Variable $CO_2/N_2/He$ Mixture with a 1 μs Excitation Length	59
4.4	Magnetic Field Effects On a Border-line Unstable Plasma	60

List of Figures

Figure		Page
1.1	Energy-level diagram of an idealized three-level laser.	5
1.2	Energy-level diagram of an idealized four-level laser.	5
1.3	Resistively ballasted pin discharge schematic.	10
1.4	UV preionized, transverse discharge schematic.	10
1.5	Regions of a gas discharge.	11
1.6	Excitation geometries used in e-beam pumped lasers	13
1.7	Electron beam stabilized excitation geometry.	13
1.8	Vibrational motion of CO_2	16
1.9	Energy level diagram of CO_2	16
1.10	KrF discharge map.[13]	20
1.11	Potential energy diagram of KrF.	23
2.1	Pulsed Electromagnet.	27
2.2	TEA Discharge Structure.	29
2.3	TEA Discharge Electrical Schematic.	30
2.4	Modified TEA Discharge System.	32
2.5	Photograph of the Modified TEA Discharge System.	33
2.6	Modified TEA Electrical Schematic.	35
2.7	Rail Gun TEA Geometry.	37
2.8	Rail Gun TEA Electrical Schematic.	38
3.1	Derived Distribution Functions of Electrons.[20]	43
3.2	Drift Trajectories and Distances.	49
3.3	Raether Breakdown in Pulsed Discharges.[22]	52
3.4	Thermal Instability Formation Time.	55
4.1	V-I Characteristics of a 12:14:74 $CO_2/N_2/He$ Mixture from 250-500 torr, with Magnetic Fields from 0 to 0.41 T.	61

LIST OF SYMBOLS

B	Magnetic Induction
d_c	Cathode Fall Distance
E	Electric Field
E_l	Energy of Lower Laser Level
E_L	Energy of a Molecular Level
E/N	Electric Field to Gas Density Ratio
g_0	Small Signal Gain
k_b	Boltzmann Constant
l	Angular Momentum Quantum Number of CO_2
m_n	Mass of a Single Molecule 'n'
N	Gas Density
N_n	Neutral Gas Density
n_D	Discharge Efficiency
p	Gas Pressure
$Q_{n\text{-}mix}$	Collision Cross Section for Neutral to Gas Mixture Collisions
T	Temperature
T_n	Neutral Gas Temperature
TEA	Transversely Excited Atmospheric pressure
u_x	Velocity in the E x B Direction
u_y	Velocity in the E Direction
β_n	Hall Parameter of species 'n'
v	Vibrational Quantum Number of N_2
v_1	Asymmetric Vibrational Quantum Number of CO_2

LIST OF SYMBOLS

ν_2	Bending Vibrational Quantum Number of CO_2
ν_3	Symmetric Vibrational Quantum Number of CO_2
ν_{m-n}	Momentum Transfer Collisional Frequency of Species 'n'
ω_{c-n}	Cyclotron Frequency of Species 'n'

1. INTRODUCTION

Since the invention of pulsed lasers, research has been active in the areas of long pulse, high power and high repetition rates. In addition, new laser systems have been developed, making pulsed optical energy available in solid, liquid, gas and semiconductor materials. A most recent development of these pulsed laser systems, the excimer laser, has created new applications in laser isotope separation, microsurface etching, UV lithography and laser surgery. Even with this rapid development of new applications, further uses for the excimer laser are somewhat limited, since the optical pulses presently available are typically less than 50 ns in duration. However, if the duration of the optical pulse could be increased a number of important benefits would be realized. In particular if lower power levels are attainable, then optical fibers can more effectively be employed in the beam delivery system. Once optical fiber transport is achievable, the excimer laser system will attain the additional and very important benefit of ease of use.

The initial purpose of this thesis research project was to fulfill the purpose of developing long optical pulse excimer devices, by utilizing magnetic fields to stabilize the laser plasma; such that uniform extended duration electrical excitation of the active media can be achieved. The process by which this effect is accomplished has been termed "Magnetic Stabilization". In this chapter, a description of how this process can be effective in enhancing the stability of a gas discharge will be explained. Following this, the motivation for the application of this technique to excimer lasers will be given. This follows with a brief introduction into the lasing process and a historical development of pulsed lasers will provide basic background to both the invention and development of these useful devices. To complete the introduction, a detailed description of the carbon dioxide and krypton fluoride lasers will give information required for an understanding of how these particular lasers systems operate.

1.1 The Magnetic Stabilization Concept

The use of magnetic fields to stabilize laser gas discharges has been established as a viable process in the electrical excitation of continuous wave CO_2 laser systems. Past experimental and theoretical work,[1,2,3] has shown that the magnetic stabilization process works by suppressing electrothermal discharge instabilities in CO_2 laser gas mixtures. The principle stabilizing mechanism appears to be associated with a "smearing out" of local hot spots. This process has been shown to be due to the Lorentz **E** x **B** force experienced by charge carriers when a radial, or transverse, magnetic field is applied between the anode and cathode. If the electric field is in the z direction, and magnetic field is in the r direction, then the resultant force experienced by an electron will be $\mathbf{F} = qE\underline{z} - qvB\underline{\theta}$. The ensuing motion of the charge carriers will then be in a helical pattern approaching the anode or cathode. The net effect will be the deflection of the charge carriers, primarily the electrons, from their normal direct trajectory. This deflection results in a "sweeping" out of any locally dense electron concentrations. Since the rotational motion caused by the electron drift is different for each different electron velocity, this effect smeares the charge carriers into a more uniform density. As such, the process can in principle delay the eventual growth of a thermal instability, which normally occurs within a period of $\simeq$ 1 ms in a CW CO_2 discharge.

Extensive theoretical and experimental study has documented that only modest field strengths of several hundred gauss are needed for sufficient mixing of a low pressure, 30 torr, CO_2 discharge. The magnetic field strength necessary for stable operation in higher pressure systems is much different. This follows from the fact that two pressure related conditions must be met for stable discharge operation. These are the instability length and the instability time of formation. The instability length is the transverse distance a charge carrier must travel in order to guarantee that the secondary emission of an electron from the cathode surface travels in a path different from the previous electron. If this condition is not satisfied, then when an electron suffers an ionization collision above the cathode surface, the resultant positive ion could, upon hitting the cathode surface, induces an electron travelling in the same path as the previous electron. This effect correspondingly increases the conductivity of that

path; and in a short time streamers and arcs can result. The instability formation time is the time for a glow-to-arc transition to occur. In higher pressure gas mixtures both of these values decrease. This aspect thereby results in the need for higher magnetic field strengths to stabilize discharges at higher pressures. For a 700 torr CO_2 system, magnetic fields of several thousand gauss are expected to be required, in order to achieve stable discharge operation.

1.2 Motivation

The magnetic stabilization concept has been utilized in a variety of excitation geometries to stabilize gas discharges. The thrust of the research project outlined in this thesis is to advance this technique into the regime of pulsed laser discharges.

The first experimental application of these magnetic fields was to convectively cool the gas by rotating the discharge with the use of static magnets[4]. This approach was found to be too slow for bulk gas motion, so it was subsequently applied to charge carrier motion. An initial demonstration of this modified concept was realized in the MAGPIE laser geometry[1]. This system used a radial electric field and a longitudinal magnetic field to create an **E** x **B** drift for electrons and ions. The process was shown to stabilize the discharge such that a much higher power level could be sustained with a magnetic field, than that which could be achieved in its absence. These initial transverse discharge results served as further motivation for studying the effects on axial discharge configurations.

The axial system used a longitudinal electrical field and a rotating magnetic field perpendicular to the electric field, to create the **E** x **B** Lorentz drift[3]. The rotation rate of the magnetic field was 60 Hz, and it was soon observed that this field stabilized the discharge by moving the discharge column in an annular region at the same 60 Hz repetition rate. Laser action in a hot plasma $\simeq$ 400 °C was subsequently achieved by having the stimulated emission follow a channel which was previously cool.

The achievement outlined above inspired research to further extend the magnetic stabilization technique into the realm of high pressure lasers. The major foreseeable challenge in this effort was expected to be the creation of sufficiently strong magnetic fields to drive an

electron drift capable of quenching plasma instabilities; thereby effectively extending achievable excitation times. If successful, this process will be applied to CO_2 TEA lasers and then to the KrF and XeCl excimer lasers.

1.3 Historical Development of Pulsed Lasers

Since the development of pulsed lasers is an ongoing process, a brief introduction into the historical advancement of these devices will be given. In so doing, a short description of the laser process will explain how stimulated emission is possible. Following this, recent advances in solid state and gas lasers will be presented, ending with a discussion of the TEA CO_2 and excimer lasers.

1.3.1 Three and Four Level Lasers

Lasers are usually classified as 3 or 4 level devices. The difference between these two types is a consequence of how many energy levels are involved in the excitation process. For lasing action to occur a "population inversion" must be generated. In this context a larger excited state density exists in a higher lying energy level, than that in a corresponding lower energy state. In a 3 level system a depletion of at least 50% of the ground state must occur in order to create a population inversion. This follows from the fact that the lower laser level is also the ground state. An energy level diagram of such a 3 level laser is shown in Figure 1.1. In contrast a 4 level device, shown in Figure 1.2, has its lower laser level separated from the ground state by an energy $E_1 \gg k_b T$, where k_b and T are respectively the Boltzmann's constant and the ambient temperature of the bulk gas. Consequently, in such a system thermal population of the lower laser level can usually be neglected. A population inversion is thereby created as soon as the upper laser level, E_2, becomes populated. Because of the fact that its lower level is unpopulated, a 4 level laser requires a much lower pumping density in order to reach a lasing threshold, than does a 3 level device.

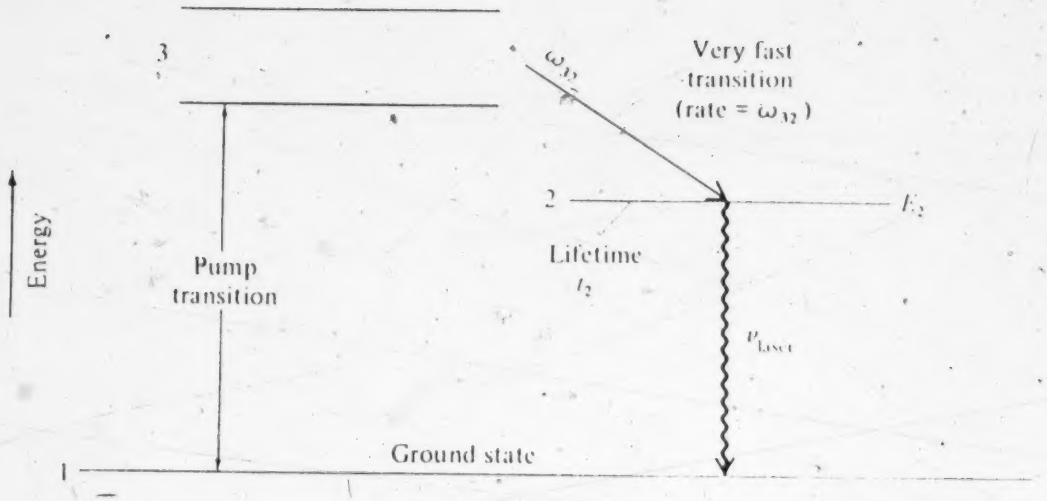

Fig. 1.1 Energy-level diagram of an idealized three-level laser.

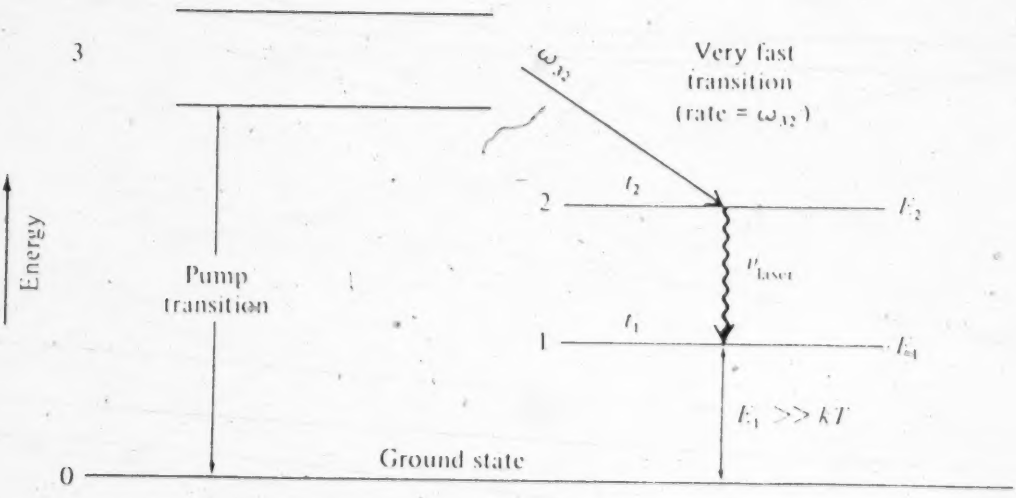

Fig. 1.2 Energy-level diagram of an idealized four-level laser.

1.3.2 Solid State Lasers

The very first laser to be developed was the ruby laser. This unique device was demonstrated by T. H. Maiman[5] at the Hughes Research labs in Malibu California in 1960. The initial unit was a pulsed device, capable of delivering peak powers in the kilowatt range, and total energies of several hundred millijoules. The ruby laser, like most other subsequent solid state lasers, used optical pumping to create a population inversion. However, since the ruby is a three level laser, intense pumping is necessary to create an inversion. Once achieved, lasing action originates between the ^2E and $^4A_2$ bands. Consequently, stimulated emission occurs between these bands at two wavelengths, of which 694.3 nm is the strongest. After the initial demonstration of the feasibility of the "lasing concept", many other solid state laser systems were soon developed.

The Nd^{3+} ion was soon recognized to be a potential laser candidate, and in 1961 Johnson and Nassau[6] achieved stimulated emission of Nd^{3+} in a $CaWO_4$ host matrix. Initially this first Nd device was only able to lase for a few seconds, but a year later CW operation for up to an hour was achieved. This long period of operation was due to the fact that the Nd^{3+} ion is a four level laser; thus much lower pumping densities were found to be adequate for CW performance. In the following years, Nd^{3+} impurities were introduced into a variety of host crystals, which provided laser activity. It was not until 1964 however, that Geusic *et al*[7] showed that YAG was the most promising material for low power threshold laser emission. In 1961 Snitzer[8] also found that Nd^{3+} atoms doped in crown glass, in the form of rods or fibers would also lase. In general, high pulse energies are easier to achieve in amorphous glass rod devices, than in single crystal lasers. The reason is that the isotropic properties of the glass host make it possible to dope the Nd^{3+} in higher concentrations, while still retaining excellent optical uniformity. Even though CW action is possible with Nd^{3+} in either YAG or glass matrices, the later is not generally used in the CW mode; since the power threshold for the YAG crystal is considerably lower. A low threshold makes it easier to run laser devices in a continuous manner.

1.3.3 The CO_2 Laser

The CO_2 laser was initially developed by Patel[9] in 1964, as a continuous wave laser. However, due to its comparatively large quantum efficiency, this device was soon utilized in the pulsed mode, to create an efficient, high peak power laser. In the late 60's to early 70's French[10] and Canadian[11] scientists perfected a transverse excitation technique, which permitted the operation of a CO_2-N_2-He discharge at much higher pressures. Ultimately operation at atmoshperic pressure created the *transversely excited atmospheric* or TEA laser. With this new system, peak powers in the megawatt range were easily obtainable; with electrical efficiency in excess of 10%.

1.3.4 The Excimer Laser

A new type of pulsed laser came into existence in 1970. This device used the principle of a unbound or zero population ground state to achieve stimulated emission. These lasers were initially called *rare gas dimers*, but were latter just termed *excimer* lasers. Rare gases as well as H_2, O, Ne, Cd, C, and rare gas combinations such as Ar-N, or He-N were used in these devices. The most successful of these combinations, called the rare gas halides, include ArF, KrF, XeF and XeCl. The ever increasing commercial success of these rare gas halides is due to the fact that they are able to efficiently produce very short wavelength UV radiation.

1.4 Methods of Excitation

Laser excitation can be achieved by several methods, of which optical, self-sustained electric discharge, ionization and thermal pumping are the most common. In general, one or another of these processes is preferred, depending on the particular laser system in question. As an example, optical pumping is used almost exclusively for solid state and liquid laser systems, although it can also be used for gas lasers as well. Self-sustained electric discharges on the other hand, are used only for gas laser systems and then primarily with low pressure systems. For high pressure gas lasers, ionization pumping is more commonly used. The process relies on high energy free electrons to transfer energy into the gas mixture through

ionization collisions. Lastly, thermal pumping is occasionally employed in gas lasers; but is generally restricted to vibrational excitation of lower energy molecular gases. Given below is a description of various excitation techniques.

1.4.1 Optical Pumping

Optical pumping is based on the creation of an active media through absorption of radiation from an intense light source. The light source can be another laser, or more often a gas "flash lamp" discharge. The advantage of optical pumping, over other techniques, arises from the fact that it is possible to obtain a single light source with a spectrum that closely matches a single excitation level, or group of levels in an atom. This results in selective pumping of the upper laser level, and its nearby levels. As a consequence of this, nearly 100% of the optical energy can be transferred into populating the upper laser level. In the case of the Nd^{3+} : YAG laser, laser diodes have recently been used to efficiently couple energy into the Nd^{3+} absorption band.

Since optical pumping is effective only for optically allowed transitions, this implies that radiative decay from the pump level can be a problem in depopulating the pump level. Therefore, for a population inversion to be created it is necessary that a metastable state lie close to this optically pumped level. Efficiencies achievable with optical excitation depend both upon the light source and quantum efficiency of the laser. For flash lamp pumped Nd^{3+} laser systems, 3-4% efficiencies are typical. However, with diode pumped systems, efficiencies of 70 to 80 % are theoretically possible.

1.4.2 Pumping with Self-Sustained Electric Discharges

Self-sustained electric discharges, also known as avalanche discharges, can be used for CW laser pumping in rarefied gaseous mixtures at pressures in the 1-50 torr range or for pulsed laser operation of up to several atmospheres. In addition, electric discharge pumping provides the most effective method for long term CW operation of gas lasers.

An avalanche discharge relies on the creation of a plasma, generated by an externally impressed electric field, exciting the laser mixture via collisional energy transfer of electron energy, gained from the electric field, to the active species. A schematic diagram of an avalanche discharge system, shown in Figures 1.3 and 1.4, employs either resistively ballasted multi-element pins, or single element shaped electrodes, such as the Chang or Rogowski profiles. As shown in these figures, avalanche pumping uses the electric field to provide both ionization and excitation. The bulk of the ionization is created in a region known as the cathode fall; while most of the excitation occurs in an adjacent zone called the positive column. These regions of a gas discharge are shown in Figure 1.5, where the cathode fall distance is depicted by d_c. A noticeable characteristic of the cathode fall is that it always has a voltage drop of a few hundred volts. In addition, the product of the cathode fall distance and gas pressure (pd_c) is given by a gas dependant constant.

In a self-sustained discharge, an optimum ratio of the electric field to gas density ratio given by E/N, which is related to the electron energy and hence laser excitation efficiency, is not readily attainable. One method of adjusting this ratio is to vary the concentration of the buffer gas; usually He. In the case with TEA laser discharges, even if an optimum E/N ratio is attained, short high current electrical pulses are still necessary for self-sustained operation. This requirement necessitates the use of a low inductance circuit, in order to achieve arc free performance. In fact, a minimum level of inductance is always sought since the systems stability depends greatly on the rise time of the current pulse.

There are several methods by which power may be supplied to the discharge chamber, among these are Blumlein circuits with strip transmission lines, charged coaxial cables, lumped element transmission lines, and capacitors. Switching is achieved most simply with the use of a spark gap. Other possible methods of switching are achieved using thyratrons, impulse charging of the power supply, or allowing the power supply to ring up to the gas breakdown voltage.

Often the plasma is initiated by weakly ionizing the bulk gas, through the use of radioactive, X-ray, or UV radiation sources. Radioactive preionization is achieved from the

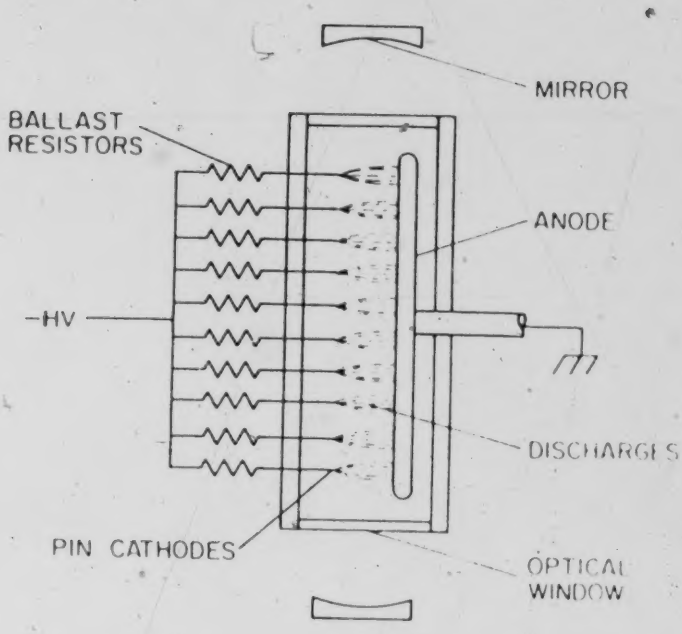

Fig. 1.3 Resistively ballasted pin discharge schematic.

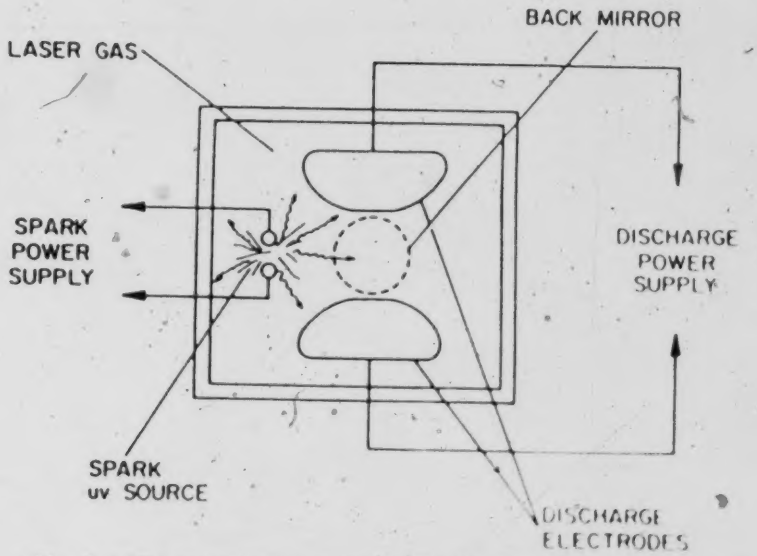

Fig. 1.4 UV preionized, transverse discharge schematic.

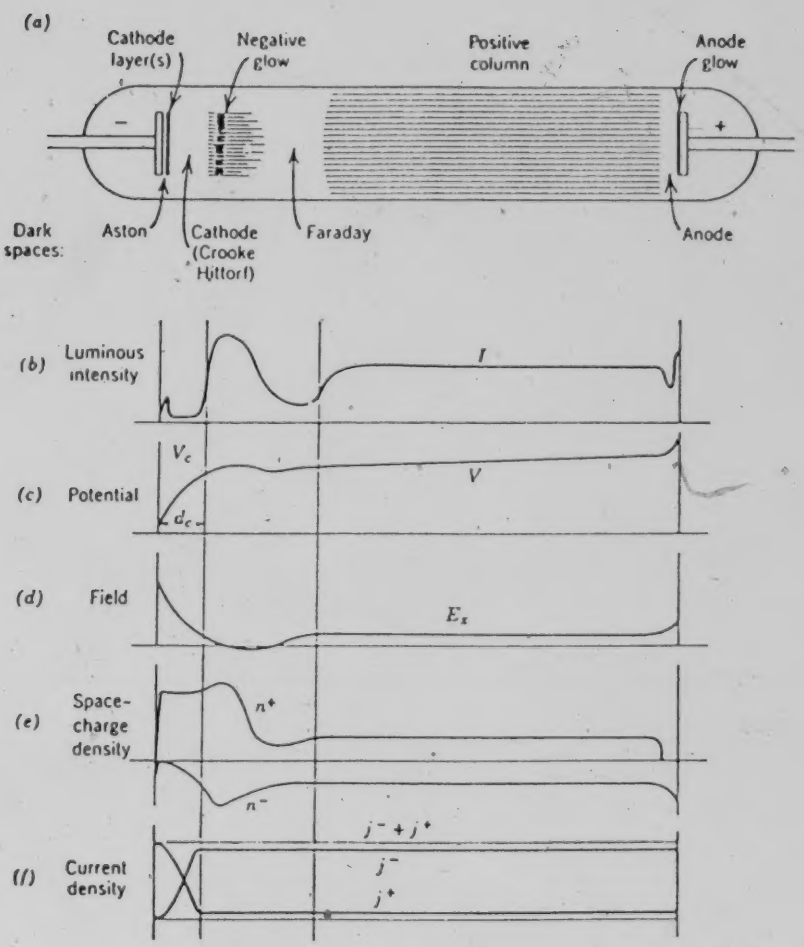

Fig. 1.5 Regions of a gas discharge.

decay of a nucleus, which in turn ionizes the gas through collisions with the decay particle. X-rays, usually used in a pulsed mode, are employed for the preionization of large aperture laser chambers of up to 15 cm. This follows from the fact that the high energy photons have a smaller cross section, thereby providing a deeper penetration into the laser volume. The simplest of the preionization techniques is ultraviolet irradiation, often produced by small corona discharges, spark gaps, or by semiconductor spark arrays. However, due to its larger absorption cross section, the UV penetration depth is reduced to $\simeq$ 10 cm. This process of preionization has also been shown to greatly improve the uniformity of gas discharges.

1.4.3 Ionizational Pumping

For high pressure laser excitation, pumping by self-sustained electric discharges is generally not easy to achieve, due to arc formation and the occurrence of discharge instabilities. To overcome this problem, high energy electron beams have been employed to ionize the gas by free electron impact. Excitation geometries using this technique are shown in Figure 1.6. The generation of these electron beams (e-beams) is generally accomplished with large capacitor banks charged from 0.1 to 2 MeV. The electron beam is then accelerated in an evacuated channel through a semi-transparent anode made of Titanium foil. This foil transmits the e-beam into the discharge chamber, with current densities of up to 500 A/cm^2. At pressures of 1 atmosphere or greater, this 25 to 50 μm thick foil must be supported by a rigid grid, yet typical transmittance is in excess of 50%.

In these systems all the energy required for ionization and excitation comes from the e-beam; thereby eliminating the problem of arc formation that occurs with avalanche discharges. If an electric field is also used in conjunction with the e-beam, this method provides an even more efficient system. As such, the process is referred to as electroionization, or e-beam sustained excitation.

1.4.3.1 E-Beam Sustained Excitation

A schematic of an e-beam sustained excitation geometry is shown is Figure 1.7. In such a system an electric field is applied across the discharge chamber to provide the

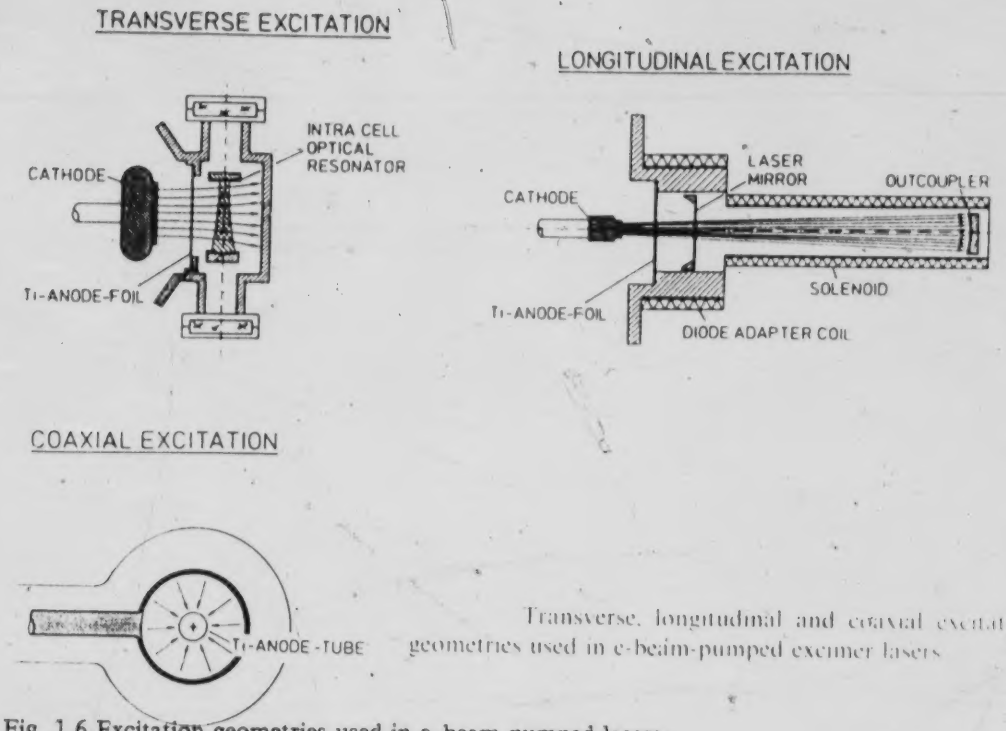

Transverse, longitudinal and coaxial excitation geometries used in e-beam-pumped excimer lasers

Fig. 1.6 Excitation geometries used in e-beam pumped lasers

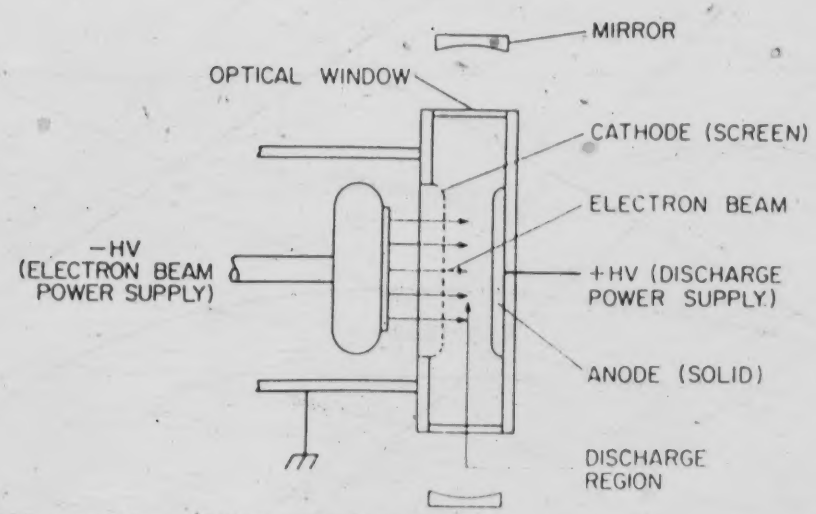

Fig. 1.7 Electron beam stabilized excitation geometry.

optimum E/N ratio. Thus by using an e-beam to provide ionization, and an auxiliary electric field to run the discharge, the excitation process becomes decoupled from the ionization process. In this manner the pumping electric field becomes independent of pressure. In general it is found that at the optimum ratio of E/N, the electric field is too weak to create sufficient electrons to maintain a self-sustained discharge; thus the need for the e-beam. As a consequence of these factors, electron beam stabilized systems are potentially more efficient than direct excitation e-beam systems. This follows since the e-beam provides a homogeneous ionization background and high pressure stable discharges can be maintained without encountering many of the problems that occur with avalanche discharge systems. In addition, the use of an electron beam provides an effective means to overcome the non uniform excitation problems that occur with direct e-beam devices.

The process used to generate the e-beam in this case is similar to that employed in the direct e-beam systems, except that the e-beam energy is greatly reduced. Typically current densities are $\simeq 2$ A/cm^2, which in turn enhance the Ti foil lifetime.

1.4.4 Thermal Pumping

In thermal pumping vibrational and rotational levels of a molecule are populated by heating the gas to temperatures between 1000 and 2000 K. Since thermal population of a vibrational level is given by

$$N_{vib} = N_0 \exp[-E/k_b T] , \qquad (1.1)$$

increasing the temperature does not by itself create a population inversion. As a consequence, successful thermal pumping of a laser necessitates that two other conditions must be met. One condition is that the population density of the lower laser level must be closely coupled with the translational temperature, while the upper laser level remains relatively constant despite any fast temperature changes. The translational temperature refers to the temperature of the bulk gas.

For a molecule satisfying this condition, pumping of the upper laser level occurs from thermal heating of the gas, while a population inversion is created by the process of adiabatic expansion. This results in a depopulation of the lower laser level faster than the upper level; thereby creating a population inversion and a possible lasing condition. Lasers pumped by this method are referred to as gasdynamic lasers.

1.5 Gas Kinetics of The CO_2 Laser

1.5.1 Vibrational Modes in CO_2 and N_2

The CO_2 molecule is a linear triatomic molecule and as such has three modes of vibration, shown in Figure 1.8. These modes and the rotational mode are represented by four quantum numbers ν_1, ν_2, ν_3, and l, which correspond to the symmetric stretch, bending mode, asymmetric stretch, and angular momentum respectively. These quantum numbers are generally written in the form $(\nu_1\nu_2^l\nu_3)$ which completely specifies the vibrational and rotational state of the CO_2 molecule. Nitrogen on the other hand, is a molecule of only two atoms. Hence only one mode of vibration, specified by a single quantum number, ν, is required to fully describe its excitation state.

1.5.2 Excitation and Relaxation of the CO_2 Laser

The energy level diagram appropriate to the carbon dioxide laser is shown in Figure 1.9. It is obvious from this diagram that the CO_2 system operates as a four level laser, since the ground state is not the lower laser level.

Pumping of the upper vibrational level is achieved by either direct electron impact excitation of the CO_2 molecule, or by resonant energy transfer from excited nitrogen molecules. The excitation cross section for N_2 is $\simeq 3 \times 10^{-16}$ cm^2, while the cross section for direct impact excitation of the CO_2 upper and lower laser levels are essentially equal at $\simeq 6 \times 10^{-17}$ cm^2. Thus the excitation cross section for N_2 is 5 times higher than any of the three CO_2 modes of vibration. Consequently, N_2 is excited more readily. As a result, in typical glow

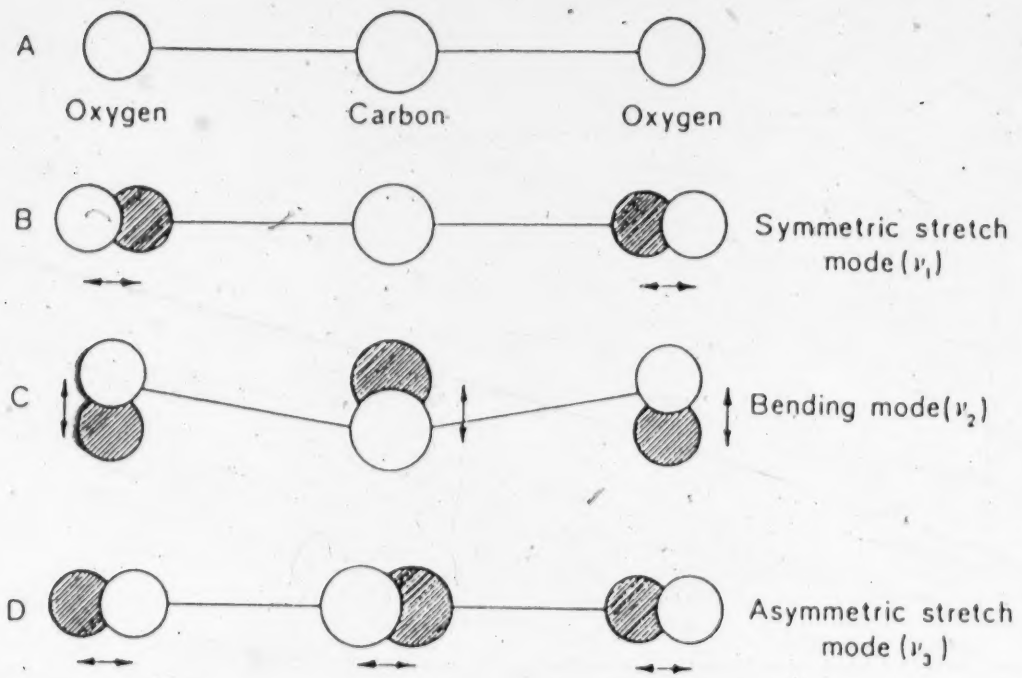

Fig. 1.8 Vibrational motion of CO_2

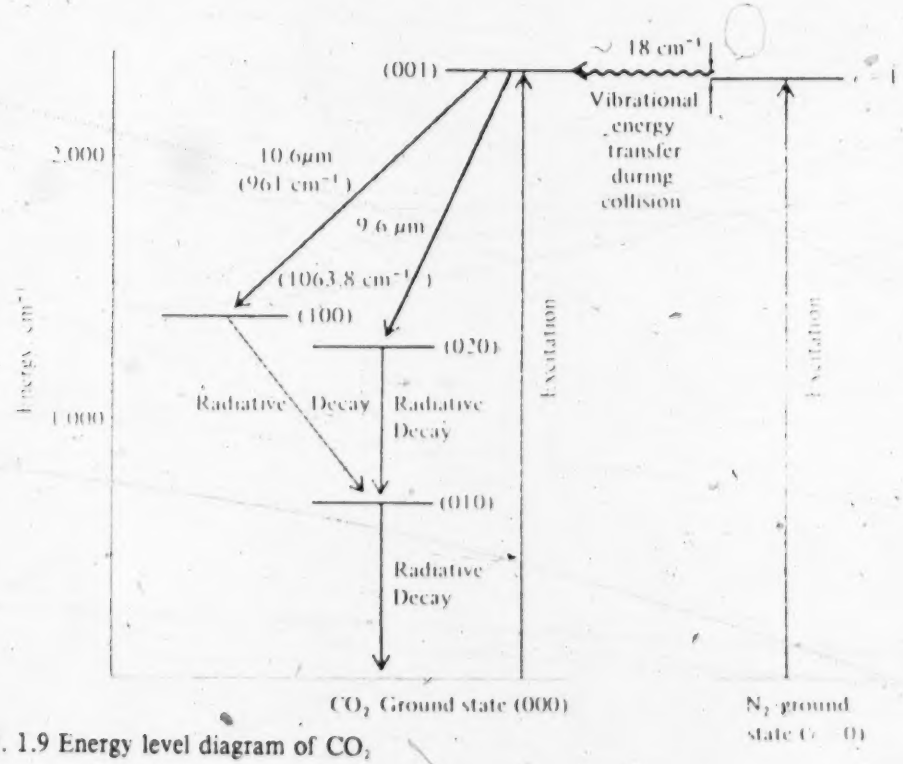

Fig. 1.9 Energy level diagram of CO_2

discharges up to 50% of the N_2 is in an excited vibrational mode. In addition, radiative decay of N_2 is forbidden, as it is a metastable state. Therefore, molecular collisions are then necessary for energy transfer to occur. Since the energy of the N_2 vibrational mode is very close to the energy of the $CO_2(00^01)$ level (differing by only 18 cm^{-1}) collisional resonant energy transfer is the primary excitation process involved in the population of the upper laser level in the CO_2 molecule. The particular energy exchange sequence is as follows:

$$e + N_2(v=0) \rightarrow N_2(v \leq 8) + (e - K.E.)\,, \tag{1.2}$$

$$N_2(v=n) + CO_2(00^00) \rightarrow N_2(v=n-1) + CO_2(00^01) - 18\ cm^{-1}\,. \tag{1.3}$$

Stimulated emission occurs between the (00^01) level and the (10^00) or (02^00) levels in the following manner:

$$CO_2(00^01) + \gamma(10.6\mu m) \rightarrow CO_2(10^00) + 2\gamma(10.6\mu m)\,, \tag{1.4}$$

$$CO_2(00^01) + \gamma(9.6\mu m) \rightarrow CO_2(02^00) + 2\gamma(9.6\mu m)\,. \tag{1.5}$$

The two lower laser levels (10^00) and (02^00) have nearly the same energy. However since $\nu_1 \simeq 2\nu_2$, these two levels are in Fermi resonance. As a consequence, a degeneracy occurs from the anharmonic forces between the two vibrations. The result is that these energy levels are shifted up and down respectively; thereby creating a larger energy separation than expected.

Relaxation of the (10^00), (02^00) lower laser levels occurs through a collisional process. Collisional relaxation of the lower laser level occurs very rapidly to the (01^10) level in the following sequence.[12]

$$CO_2(10^00,02^00) + CO_2 \rightarrow CO_2(02^20) + CO_2 \qquad k = 6 \times 10^5\ sec^{-1}torr^{-1} \tag{1.6}$$

$$CO_2(02^20) + CO_2 \rightarrow 2CO_2(01^10) \qquad k = 1.3 - 3.6 \times 10^6\ sec^{-1}torr^{-1} \tag{1.7}$$

Following this, a relatively slow relaxation of the (01^10) level occurs.

$$CO_2(01^10) + CO_2 \rightarrow 2CO_2(00^00) \qquad k = 175 - 210\ sec^{-1}torr^{-1} \tag{1.8}$$

or

$$CO_2(01^10) + He \rightarrow CO_2(00^00) + He \qquad k = 3.4 - 5.3 \times 10^3\ sec^{-1}torr^{-1} \qquad (1.9)$$

As can be seen by the respective rates, the collisional relaxation of the $CO_2(01^10)$ level is the slowest. Experiment has documented that the addition of Helium is of great benefit in increasing this relaxation rate. The presence of helium also increases the thermal conductivity of the laser gas mixture, as well as improving the discharge characteristics. For TEA lasers, helium is used primarily for its discharge characteristics.

1.6 Gas Kinetics of The KrF Laser

1.6.1 Electron Beam Pumped Excimer Systems

There are several ways to pump an excimer laser gas mixture. The most commonly used method is direct electron beam excitation. Typical electrode configurations of e-beam pumped devices were shown in Figure 1.6. Transverse e-beam pumping is primarily used, and relies on the high rates of excitation produced by energetic electrons colliding with the gas mixture (typically at a few atmospheres of Ar with 7% Kr, and 0.1% F_2), to create a population inversion. An energy deposition efficiency of up to 50%[13] is potentially attainable with e-beam systems. However in practice only $\simeq$ 10% of that energy is actually deposited into the rare gas species, thereby giving the process an intrinsic efficiency closer to 5%.

A more detailed description of the dominant kinetics at play in the KrF laser system is as follows. Initially the buffer gas, Ar, is ionized by the e-beam, producing free electrons which dissociatively attach to the fluorine forming F^- ions and free fluorine atoms. The specific kinetics of the process proceeds in the following manner:

$$Ar^+ + F^- \rightarrow ArF^* \qquad ArF^* + Kr \rightarrow KrF^* + Ar \qquad \text{or,} \qquad (1.10)$$

$$Ar^+ + Ar \rightarrow Ar_2^+ \qquad Ar_2^+ + Kr \rightarrow Kr^+ + 2Ar \qquad Kr^+ + F^- \rightarrow KrF^* . \qquad (1.11)$$

Radiative emission can occur from the ArF^* pair, which has a lifetime of 4 ns. However, due

to the high collisional frequency at this pressure, energy is exchanged to form the excimer metastable state instead. Since these excimer metastables have effective radiative lifetimes of only a few nanoseconds, very high excitation rates, (greater than 10^5 W/cm^3), are needed in order to achieve effective laser action. E-beam pumping can easily produce these elevated pumping levels. An additional advantage is that good discharge stability can still be obtained even though circuit inductance is not minimized. The disadvantages of pure e-beam systems are again their large size, cost, and complexity, as compared to those employing electrical discharges. Because of this fact, direct e-beam pumping is generally not found to be cost effective for small laser systems.

Electron beam stabilized discharges offer the potential for higher efficiencies, since a discharge is utilized to create the rare gas metastables. With a carefully controlled self-sustained discharge, intrinsic efficiencies can be as high as 40%. However in practice, efficiencies achieved with an e-beam stabilized discharge rarely exceed 10%.

A schematic of an e-beam stabilized discharge was shown in Figure 1.7, and a typical discharge map is shown in Figure 1.10. In the discharge map g_0, n_D, and N refer to the small signal gain, discharge efficiency, and the e-beam enhancement ratio respectively. The e-beam enhancement ratio is defined by the power deposited by an electric discharge divided by the power deposited by an e-beam, further use of the symbol N will define the gas density. It is evident from the KrF discharge map that an increase in efficiency is obtained by operating at high E/N values, while maintaining low electron densities and high enhancement ratios. The enhancement ratio is defined as the discharge power divided by the e-beam power. With e-beam controlled pumping, separate control over the electron density and electric field are possible. Thus, it becomes feasible under this method to obtain an efficient, high gain, stable discharge. Stability is obtained by constraining the discharge ionization to be less than half of the attachment rate. This stability condition is maintained since the e-beam is used to balance out the difference between the rate of ionization due to the discharge, and the rate of electron loss due to dissociative attachment. Disadvantages encountered with this approach are similar to those experienced with pure e-beam systems. Of which foil heating, low repetition rates

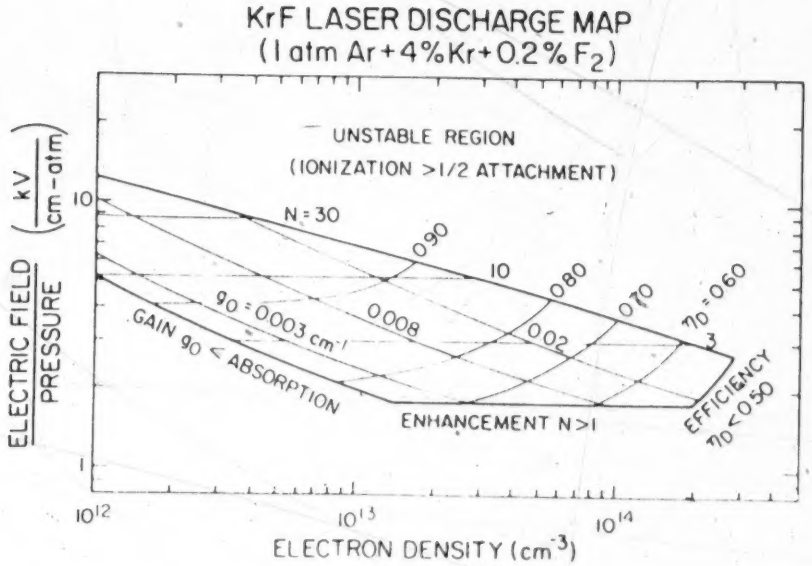

Fig. 1.10 KrF discharge map.[13]

and cost are the primary problems. However, electron beam power densities required for laser excitation need not be as high with this technique.

1.6.2 Avalanche Discharge Pumped Systems

Electric discharge pumping geometries, shown in Figures 1.3 and 1.4, offer the potential for more efficient and higher average power systems. The increase in efficiency occurs because the lower energy discharge electrons are able to pump the metastable rare gas atoms directly or through the buffer gas metastables, instead of ionizing the buffer gas and rare gas atoms. In avalanche discharge systems, it is found that He performs better as a buffer gas than does Ar. The reason is that electrons can transfer momentum through collisions more efficiently with He, than with either Ne or Ar. As a result, the discharge energy is better channeled to form the rare gas metastables by collision. These metastables combine in turn with the fluorine, forming the excimer metastable. Typical reaction kinetics for KrF are as follows:

$$e + He \rightarrow e + He^* \qquad He^* + Kr \rightarrow He + Kr^* \qquad Kr^* + F_2 \rightarrow KrF^* + F\,, \tag{1.12}$$

or

$$e + F_2 \rightarrow F + F^- \qquad e + Kr \rightarrow Kr^+ + 2e \qquad Kr^+ + F^- \rightarrow KrF^* \tag{1.13}$$

For efficient laser action, an input power density of 100 J/ℓ·μs is required, which corresponds to a discharge power of 10^5 W/cm^3. Since metastable production efficiencies in the range of 80% are possible, discharge power densities of up to 8×10^4 W/cm^3 are channeled into the rare gas metastables. Wall-plug efficiencies of 1% are feasible with this method. Higher efficiencies are more difficult to obtain, since the discharge becomes unstable with time, due to the dissociative attachment of the F_2. Such attachment, subsequently results in the collapse of the discharge impedance and eventually leads to the formation of arcs. This problem can be minimized if the current pulse is of short duration; hence the requirement for low inductance circuits.

If some form of preionization is used, the discharge will become more uniform and the glow-to-arc transition will be suppressed. This occurs because the preionization generates a weakly ionized, uniform plasma within the interelectrode volume which in turn produces secondary electrons by collision. These secondary electrons either attach to the halogen donor, stabilizing the discharge, or accelerate and gain enough energy to form the rare gas metastables.

1.6.3 Laser Emission and Relaxation of the KrF Laser

Once the KrF^* excimer is created there are several energy levels to which it can make radiative transitions. In Figure 1.11, a potential energy diagram of the KrF^* excimer is shown. Strong radiative transitions occur between the levels $D \rightarrow A\ ^2\Sigma_{1/2}$, $D \rightarrow X$, $C \rightarrow A\ ^2\Sigma_{3/2}$, and $B \rightarrow X$, the latter being the strongest transition. Dissociation of the KrF^* excimer is accomplished by stimulated emission, spontaneous emission, or by direct quenching by the halogen bearing species. Spontaneous emission lifetimes of the KrF^* excimer are typically 9 ns. Quenching by the halogen bearing species occurs in the following manner:

$$KrF^* + F_2 \rightarrow Kr + 3F \tag{1.14}$$

The laser process continues until either discharge instabilities arise, or until the halogen fuel is sufficiently depleted, thereby leading to an ionization instability. The latter arises since the recombination time of fluorine is much slower than its dissociation time. As a consequence, molecular fluorine becomes depleted during a laser discharge. Typically 25% of F_2 is dissociated in the first 0.6μs. As a result, the following reactions become less probable.

$$Kr^* + F_2 \rightarrow KrF^* + F \qquad \text{or} \qquad e + F_2 \rightarrow F + F^- \tag{1.15}$$

The net effect is a decrease in the rate of production of the KrF^* dimer, where dimer refers to any molecule with a repulsive ground state. Recombination of fluorine occurs at rates of $\simeq 10^{-32}\ cm^6 s^{-1}$. Therefore for laser gas mixtures consisting of 3 torr of F_2 in 1500 torr of He, the recombination time of F_2 is typically 21 μs. Clearly this value is much longer than the

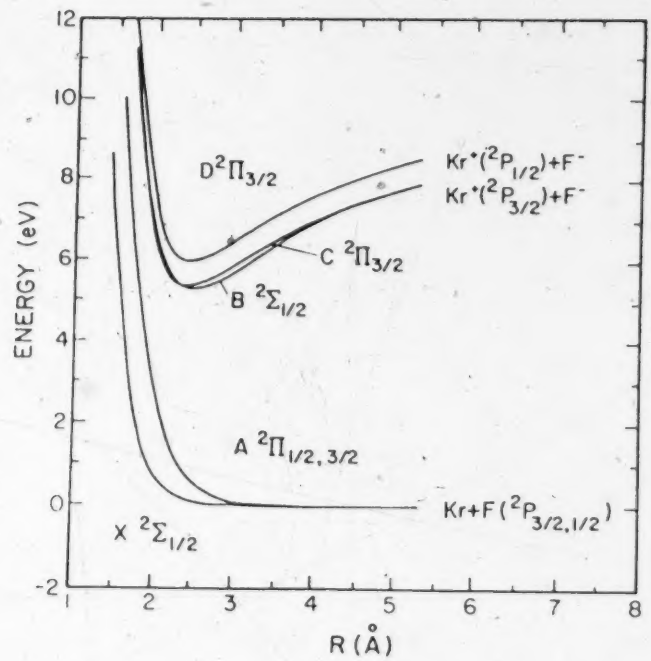

Fig. 1.11 Potential energy diagram of KrF.

discharge time. Consequently, the maximum available laser pulse energy per unit volume corresponds to at most one photon per initial halogen molecule. Typical laser gas mixtures containing 0.2% F_2 are therefore limited to output energies of 40 J for a 1 ℓ discharge volume, operating at atmospheric pressure.

2. SYSTEM DESIGN

As indicated previously, the purpose of this thesis is to investigate the feasibility of the magnetic stabilization concept in pulsed high pressure discharges. Past work[1,3,4] has documented that this stabilization process is effective in moving charge carriers[2] via the E x B drift. Furthermore, electron production and instability formation is greatest in the cathode fall area. As a consequence, this region will require the largest magnetic field, and will be the primary region of study.

Initially the system design incorporated a radial profiled magnetic field, transverse to the electric field, such that the **B** field is in the r-direction and the **E** field is in the z-direction. Since the primary area of study is the cathode, magnetic fields were profiled to be largest in this region. The charge carriers, primarily the electrons, will consequently drift in an E x B direction. This motion inhibits the formation of any instabilities by "smearing" locally dense electron areas into a more uniform concentration.

The first discharge apparatus designed to utilize this form of magnetic stabilization is called the "TEA Discharge Structure". In this system radial fields were produced by an electromagnet beneath the cathode, which also provided energy to the discharge through the cathode. This was possible since the electromagnet was connected in series with the discharge circuit.

A subsequent modification to this configuration is resulted in the "Modified TEA Discharge System". In this geometry, the electromagnet and discharge circuits were now isolated. The advantages of this approach was that separate control of the magnet made it possible to vary the magnetic field strength, while keeping the discharge electric field constant. In so doing, it was hoped that a meaningful relationship between magnetic field strength and voltage current characteristics of the discharge could be determined. In effect a higher power loading is anticipated whenever magnetic field strengths are sufficient to quench instability formation.

The last system under study is called the "Rail Gun TEA Geometry". This geometry relied on copper rails to produce transverse magnetic fields. As a consequence of this, the magnetic fields were not localized to the cathode as with the radial magnet design, but rather filled the entire discharge volume. In addition, because this geometry was similar to a rail gun it was dubbed the "rail gun" geometry. Stabilization was anticipated in this system by forcing the discharge down the rails before streamers, or arcs can form.

2.1 Pulsed Electromagnet

The design criterion of a magnet adequate for magnetic stabilization experiments, at the pressures desired, had to satisfy the requirement of producing 10,000 gauss, or 1 tesla magnetic fields, perpendicular to the electric field in the discharge. The most practical design was a pulsed electromagnet, since one tesla continuous electromagnets would imply a large power consumption and cooling system. Also, since the discharge lasts for only a few microseconds, pulsed fields are sufficient for these experiments. The original strategy was to insert the magnet into the discharge region and have it driven by the discharge current. This condition necessitates that the driving voltage be relatively low, typically a few tens of kilovolts. In order to achieve 1 tesla fields with a few tens of kilovolts, a low inductance magnet was necessary, in order to obtain peak currents sufficiently high for the production of such fields. A design which appeared to satisfy this criterion is shown in Figure 2.1. A vane structure was used to lower the magnets inductance. This structure consisted of a magnetic yolk made of mild steel, 12 copper vanes, various insulators and a brass center sleeve. A steel jacket was used as a magnetic yolk, in order to confine the magnetic field; thereby further concentrating the field strength onto the top of the magnet.

Operation of the magnet occured in the following manner. Initially the electrical pulse entered through the steel yolk to the copper vanes fastened on the yolks' outer perimeter. Following this, the current split into 12 parallel paths, as it entered the copper vanes. Each vane was insulated from each adjacent vane, as well as from the base of the yolk; thereby providing 12 individual conduction channels. These channels executed five turns around a

PULSED CATHODE MAGNET

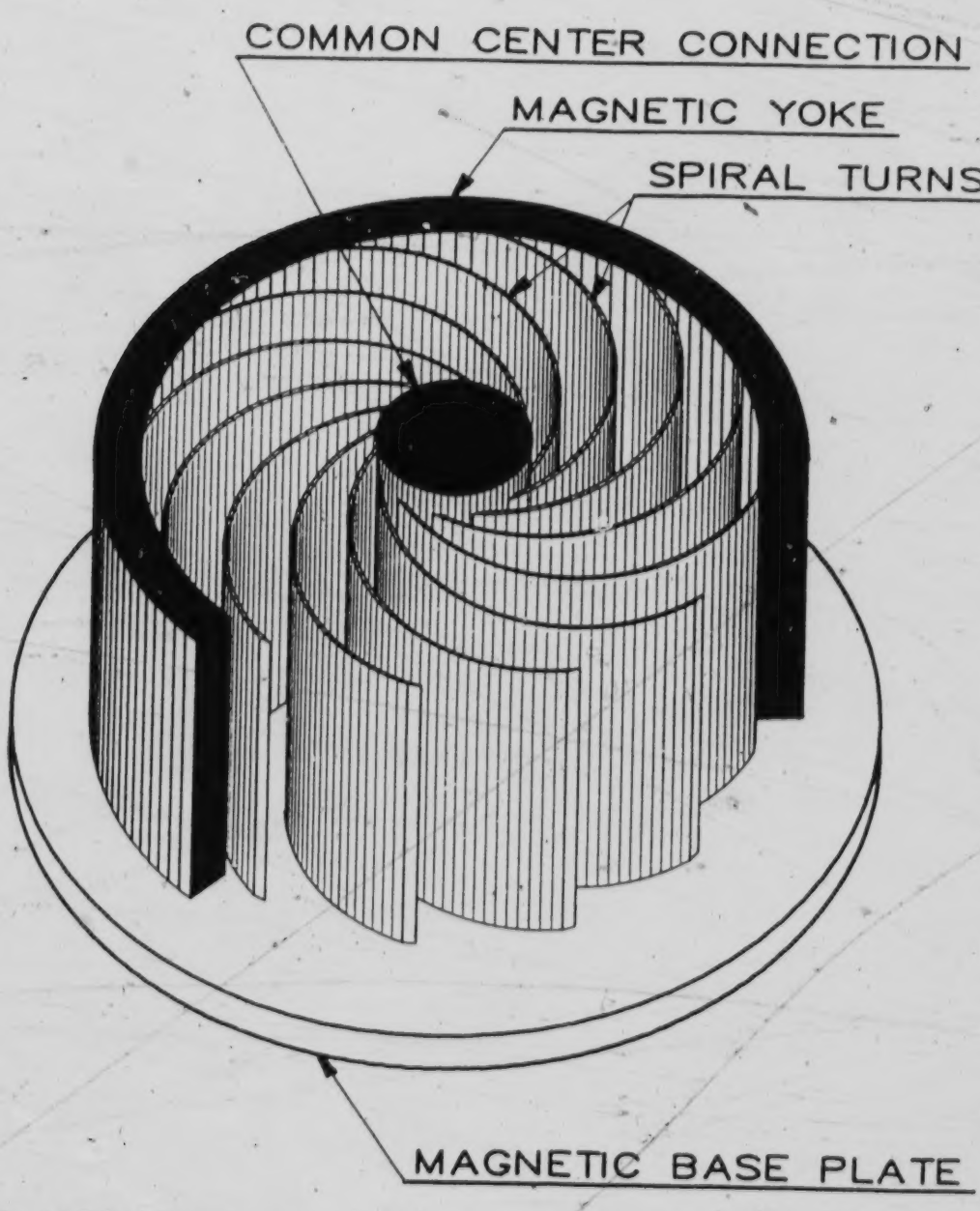

Fig. 2.1 Pulsed Electromagnet.

brass sleeve, which was connected through an insulator to the hub of the magnets' yolk. Current then flowed into the brass sleeve and continued in one of two directions. In the "TEA Discharge Geometry", the magnet drove the gas discharge via a direct electrical connection from the sleeve to the cathode. In the "Modified TEA Discharge Geometry", the magnet was separate from the discharge circuit, and the current loop was completed as the current flowed into the magnets' hub. The hub was now insulated from the body of the steel yolk, and current exited the system through a coaxial feed inserted into the base of the magnets' structure.

2.2 TEA Discharge Geometry

The vessel housing the discharge was a nominal 12" diameter plexiglass cylinder, fastened at each end by 1/2" x 14" diameter plexiglass plates, shown in Figure 2.2. The joints were sealed by 1/8 in. diameter O-rings placed in grooves slotted into these plates.

Electrical connection into the system was achieved by 1/2 in. diameter brass rods. These rods entered the system from the center of the plexiglass plates, with each rod being sealed by a swagelok fitting. Connection into the anode was made from the top, by a threaded contact into a 1/4 in. x 10 in. diameter aluminum base plate. From the bottom, the rod threaded directly into the base of the magnet.

The cathode surface magnetic field strengths initially obtained with this device were unexpectedly limited to 0.04 T[14,15,16] which were far too weak to be useful. Subsequently it was determined that the non-magnetic stainless steel cathode was responsible for magnetically screening the transient field. After several experiments, a 1.6 mm thick graphite cathode was substituted which gave much less screening, and thereby allowed cathode surface magnetic fields in the 0.4 T range to be achieved.

Once the screening problem was solved the initial system was assembled with an electromagnet / graphite cathode, and a Rogowski profiled graphite anode. An electrical schematic of this system is shown in Figure 2.3. Operation was achieved by discharging a 0.1 to 0.4 μF capacitor, switched through a N_2 pressurized spark gap. Subsequently current

TEA DISCHARGE GEOMETRY

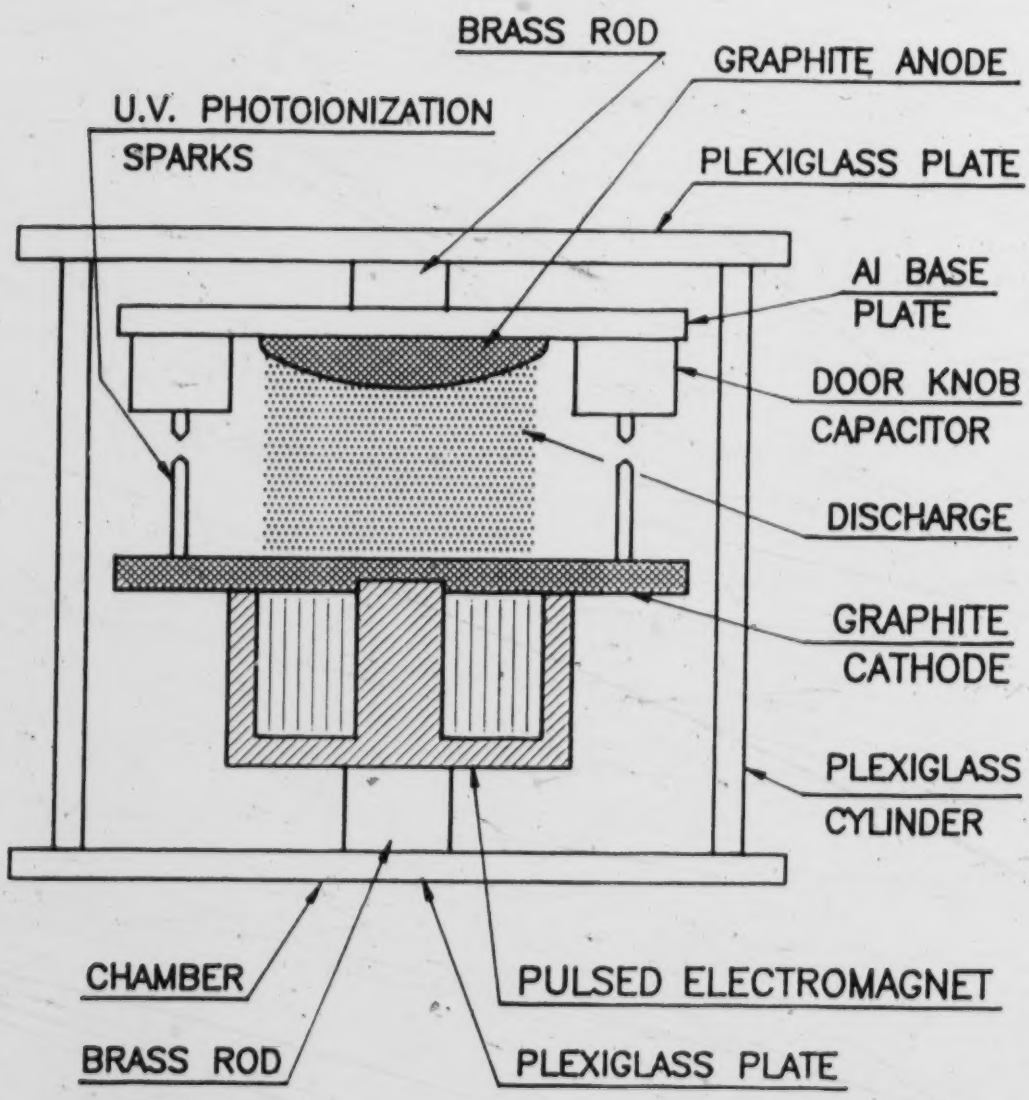

Fig. 2.2 TEA Discharge Structure.

TEA DISCHARGE CIRCUIT

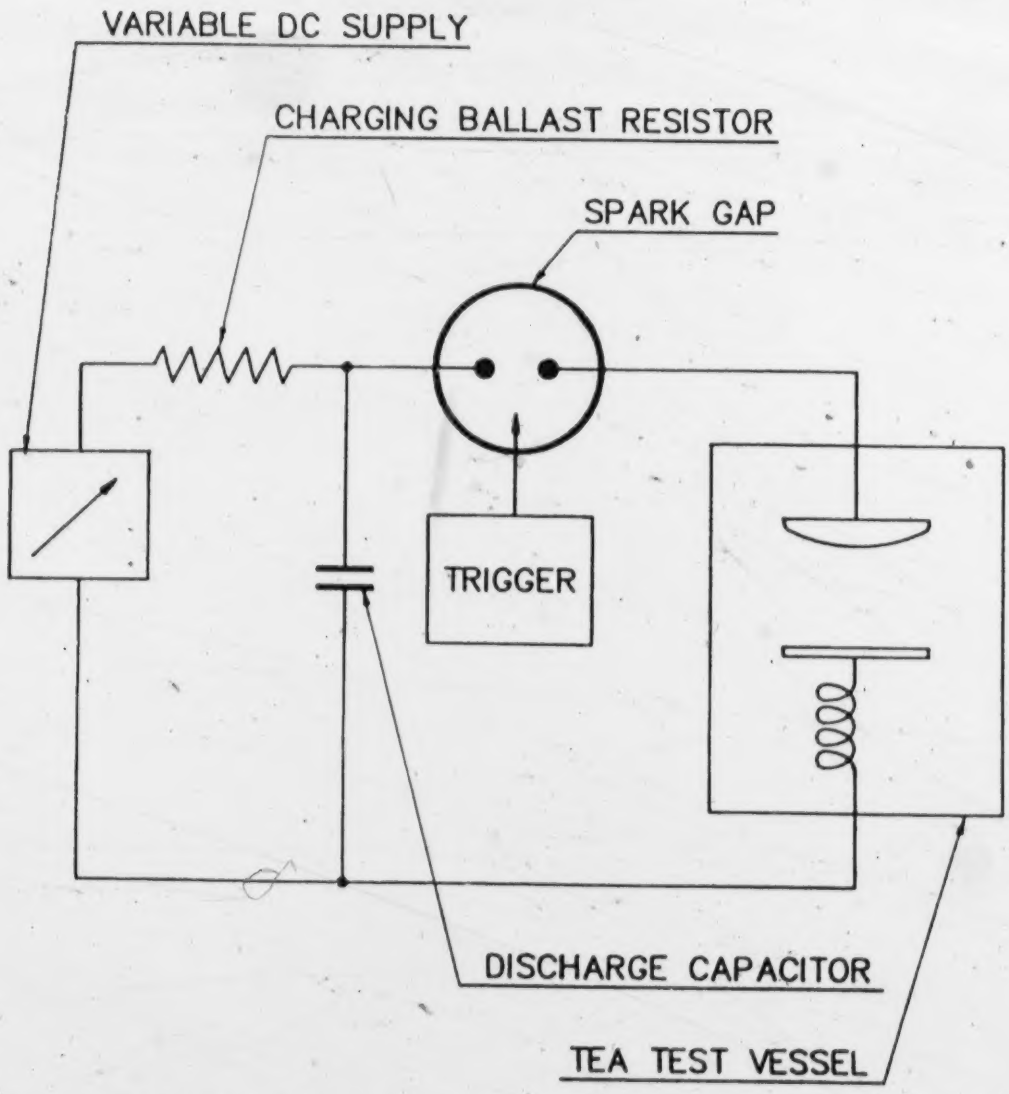

Fig. 2.3 TEA Discharge Electrical Schematic.

flowed into the circuit-initiated preionization in the laser discharge, then grew to create a strong magnetic field in the magnet. At that time the discharge became fully conducting, and the magnetic field provided a stabilizing rotational motion to the charge carriers.

The advantage with this approach arose from its simplicity, in that only one power supply and switching circuit was necessary for total operation of the system. However, as is obvious from Figure 2.3, the inductance of the discharge system was not minimized, since the magnets' inductance was added into the discharge circuit. Initial measurements of the systems inductance was 2.86 μH. However, after optimizing the external circuitry a new value of 2.03 μH was obtained. This value was still too high for stable discharge operation. To determine the magnets' effect upon the circuit, the magnet was removed and the circuits ringing frequency was measured. The result was a value of 1.38 μH, without the electromagnet installed. Even with this level of inductance, arc free discharges were not possible; therefore a modification to the system was necessary in order to lower the systems inductance still further; to within a few 100 nH.

2.3 Modified TEA Discharge System

The requirement for a low inductance circuit implied that the 750 nH magnet could not be installed in series with the discharge circuit. To overcome this problem two circuits were constructed, one each for the discharge and pulsed magnet. Restructuring the discharge into a low inductance circuit required having a very good electrical connection to and from the cathode and anode. To solve this problem, the original system was modified as shown in Figure 2.4. The central posts, which were connected to the electrodes, were replaced. A solid aluminum top plate was made, which provided the vacuum seal and also served as the mounting plate for the anode, thereby providing a solid Al conductor for the electrical connection to the anode. For the cathode connection, the plexiglass chamber was split into two sections joined to each other by an aluminum ring. This ring was mounted to the cathode, thus giving a solid Al conductor for the cathode as well. Shown in Figure 2.5 is a photograph of the actual experimental apparatus.

MODIFIED TEA DISCHARGE GEOMETRY

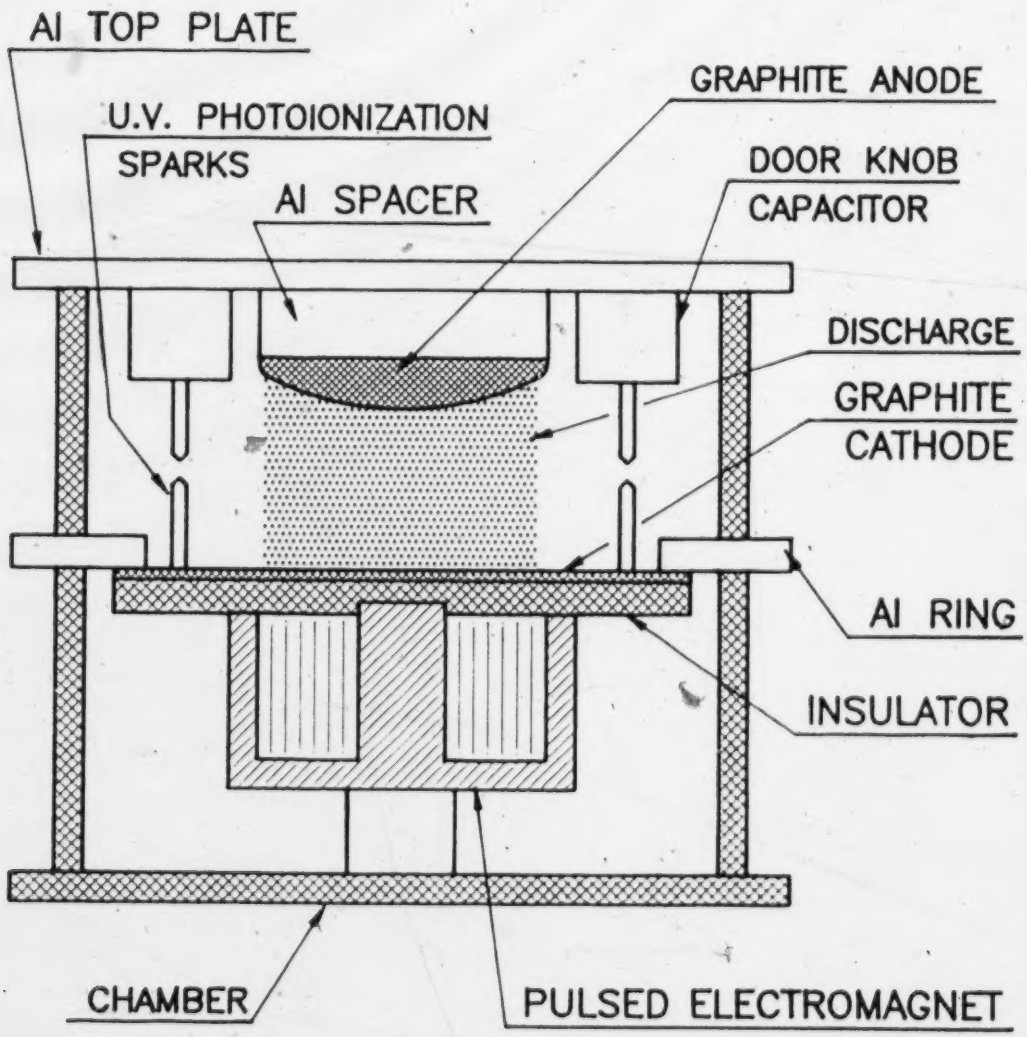

Fig. 2.4 Modified TEA Discharge System.

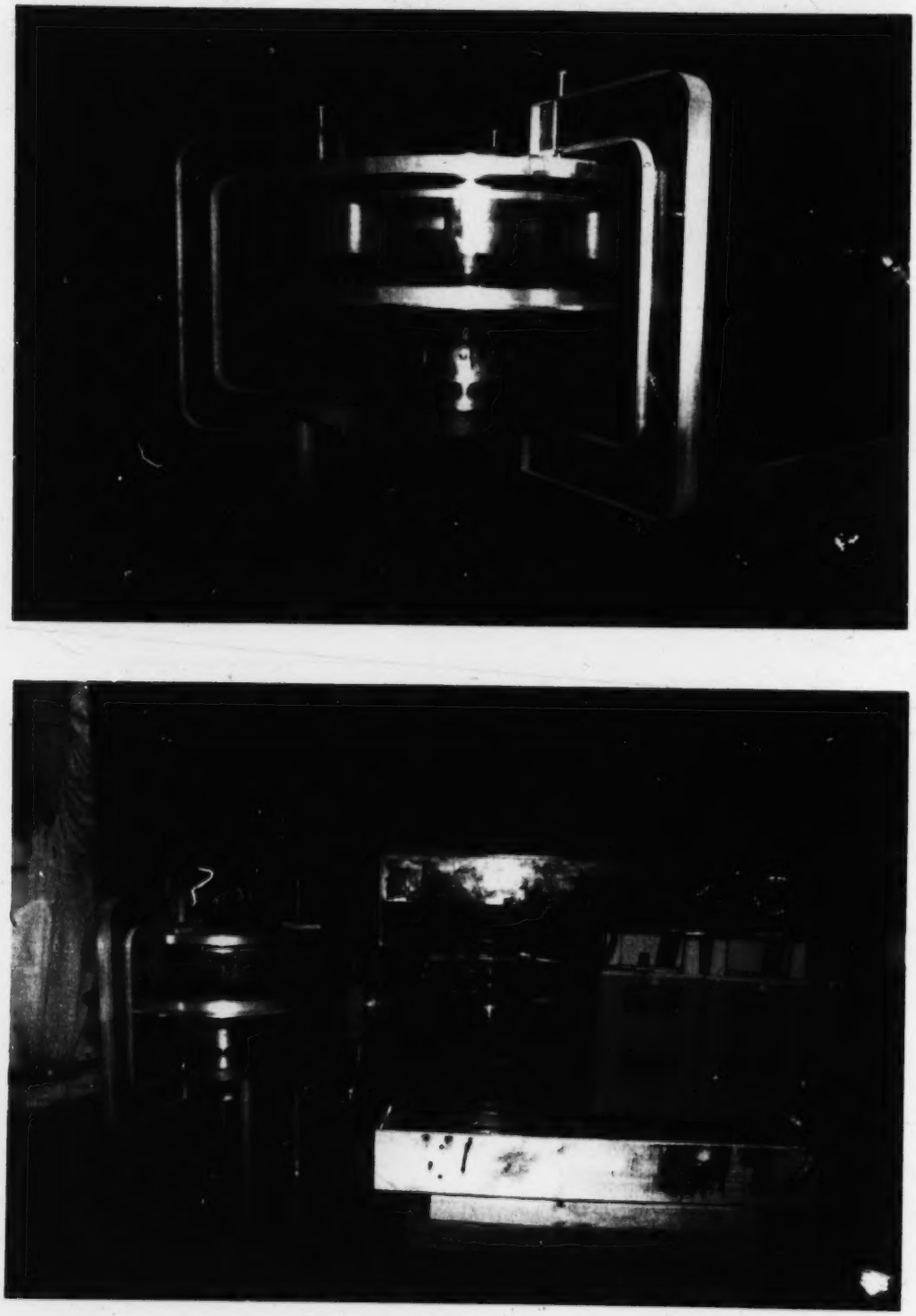

Fig. 2.5 Photograph of the Modified TEA Discharge System.

The magnet was installed just below the cathode. However, since the magnet was now a independent circuit, it had to be insulated from the cathode. This was achieved by using a 3 mm thick plexiglass plate laid over top of the magnet and insulating the two components. The new electrical schematic for this design is shown in Figure 2.6. As a result, the major challenge to this new system was to trigger the two spark gaps with only a small and reproducible delay. The need for this double trigger arose since the magnetic circuit was of higher inductance and thus required a longer 'turn on' time to reach its full strength, as compared to the low inductance discharge circuit. Several solid state delay circuits were initially tested. However, due to the large amount of radio frequency interference produced by the high voltage discharge, a solid state circuit could not be utilized. This problem was solved by using a delay trigger amplifier made by Field Emission Corporation, to trigger the spark gap directly with a high voltage pulse. A delay of 4.0 μs was used, which provided a maximum and near constant magnetic field throughout the course of the discharge. Since the two circuits were different from the previous system, new measurements of the inductances were done. The magnetic circuit recorded an inductance of 1.65 μH, while the discharge circuit was measured to be only 285 nH.

Stable discharge operation was finally observed with this system, however no stabilizing effect resulting from the presence of the magnetic field could be observed. It was thought that the modest magnetic field strength of 0.4 tesla, corresponding to a Hall parameter of $\simeq 0.1$ at 250 torr, was the source of the problem. This initiated the development of a new system, which attempted to take advantage of "rails" to produce still higher strength magnetic fields; possibly up to two tesla.

2.4 Rail Gun TEA System

This unique geometry also utilized several independent circuits to produce the magnetic and electric fields necessary for magnetic stabilization experiments. The operational principle behind this system was to create very strong magnetic fields by discharging a high voltage capacitor through copper rails inserted into the center of the electrodes. Electric field

MODIFIED TEA DISCHARGE CIRCUIT

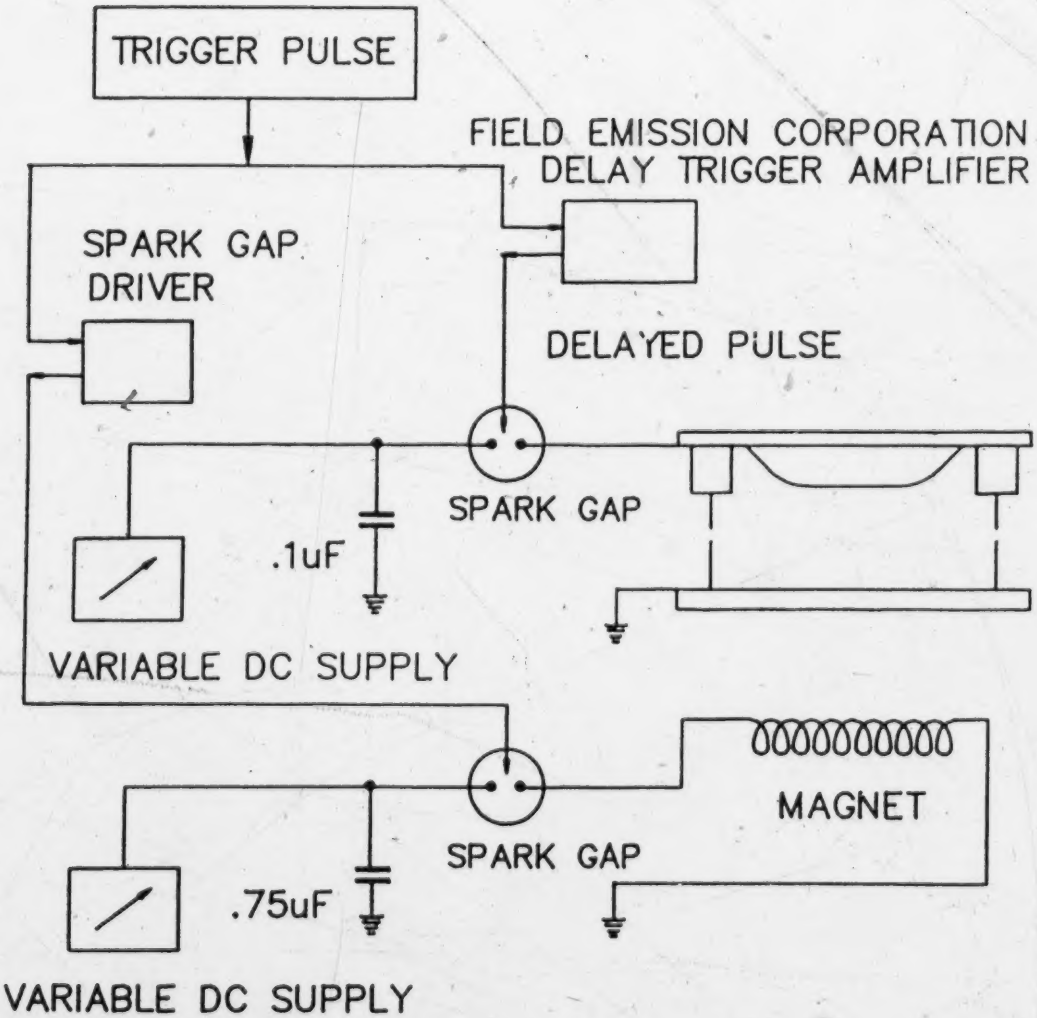

Fig. 2.6 Modified TEA Electrical Schematic.

generation was similarly produced by an independent circuit, connected between the anode and cathode. This method of field production was expected to create non uniform electric fields, due to voltage drops across the copper rails. To overcome this problem, a compensating voltage drop was initiated through a similar copper rail inserted into the anode. Thus under full operation there would be three independent circuits, two of which involved high voltage discharges across the copper rails which were inserted into the cathode and anode bodies, while the other isolated circuit drove the gas discharge.

The vessel housing the above apparatus is shown in Figure 2.7, and consisted of two aluminum plates each 17.5" x 32.5" x 5/8" in dimension, fitted to a 29.5" x 13.5" x 5/8" plexiglass vessel. Joints were sealed by 1/8" O-rings placed in grooves slotted into the Al plates.

The anode and cathode were comprised of two Rogowski profiled graphite electrodes 24 in. long, by 4 in. wide, fastened to Al plates by an Al standoff. This standoff provided a nominal electrode spacing of 2 cm. In addition, a copper rail was secured into a groove cut into the center of the electrodes by epoxy. This rail, 1.65 mm x 5.2 mm in cross section, was connected to a capacitor bank through the plexiglass walls, on the side of the vessel next to the door knob capacitors. The door knob capacitors, which provided UV preionization to the system, were located next to the electrodes.

Electrical connection into the discharge was at the end of the vessel, on the top and bottom end plates. An electrical schematic of this system is shown in Figure 2.8. For clarity the anode rail portion of the circuit has been omitted. Operation of the device consisted of discharging two circuits. The first circuit drove the copper strips, via the discharge of a 0.75 μF capacitor through 2 spark gaps. The need for the low potential side spark gap was to insulate the discharge circuit from the rail circuit. Secondly, discharging a 0.1 to 0.2 μF capacitor through a spark gap initiated UV preionization from the door knob capacitors, thereby providing a sufficient delay time for the voltage to build up across the electrodes. After this initial triggering period, uniform excitation of the gas ensued.

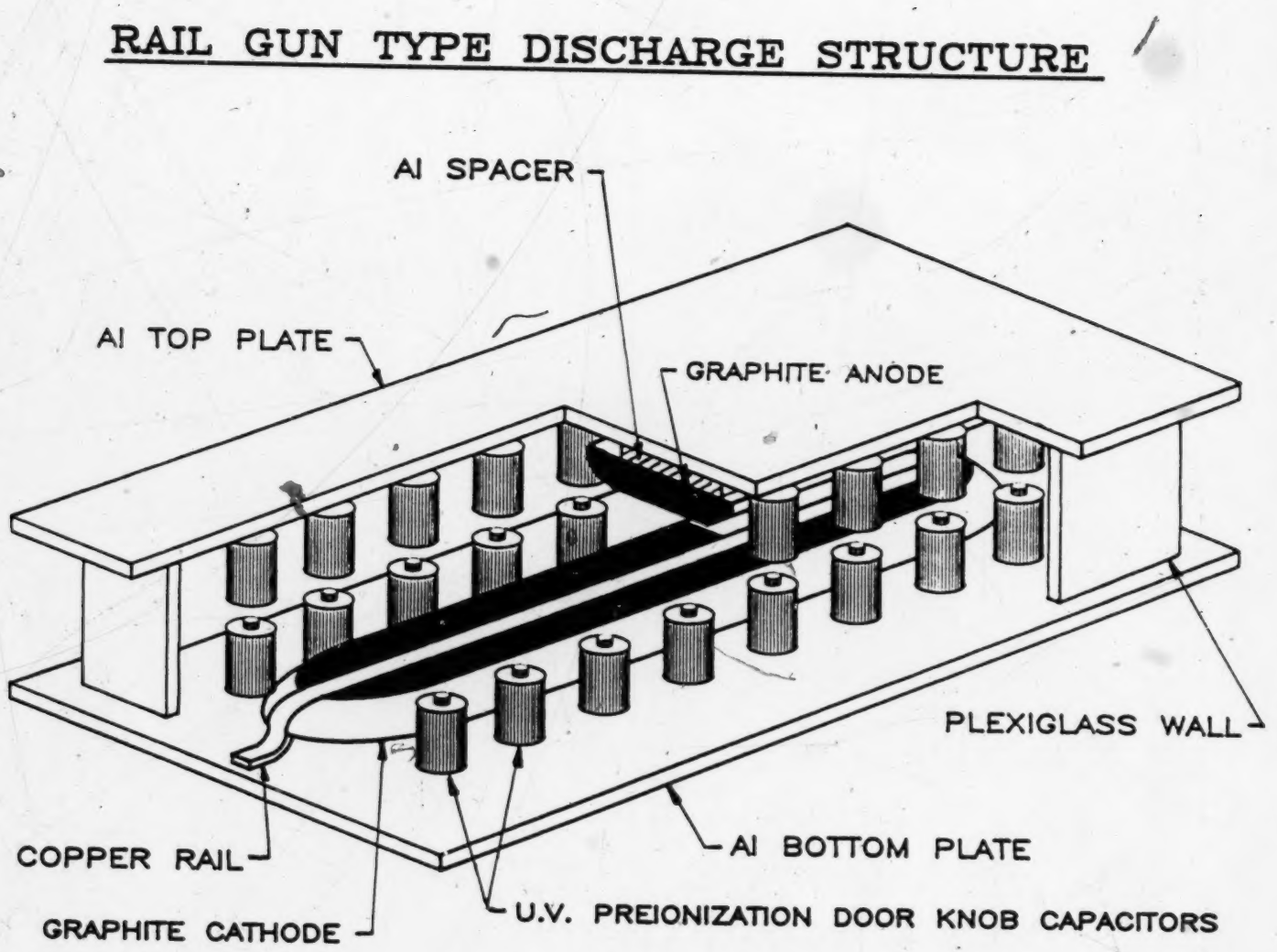

Fig. 2.7 Rail Gun TEA Geometry.

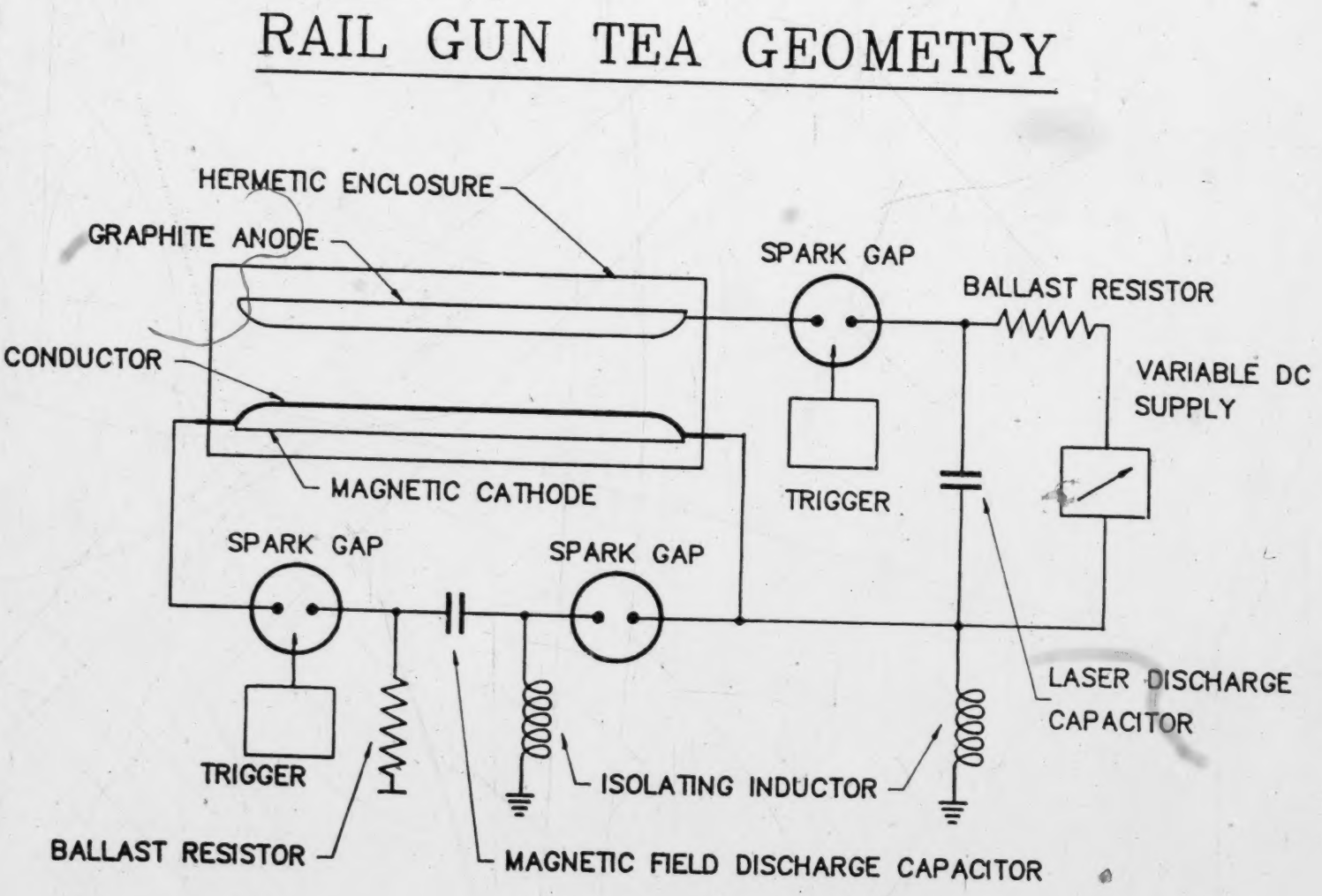

Fig. 2.8 Rail Gun TEA Electrical Schematic.

A disadvantage of this system was the high level of inductance contributed by the copper rails. This in turn created a circuit with low peak currents and the initially projected 2 tesla magnetic fields could not be realized. Thus, since a high magnetic field could not be attained, a deeper understanding of the induced magnetic drift effect was sought out, in order to determine the feasibility of some alternate means by which magnetic stabilization could be employed in a pulsed laser discharge.

3. THEORETICAL ANALYSIS

It has been shown that the magnetic stabilization concept is feasible in CW laser systems operating at pressures near 30 torr, with magnetic fields of ≃ 0.04 T. Because of the success achieved in magnetic stabilization of CW systems, this process was further extended into the realm of pulsed discharges. Because of the fact that magnetic field effects, specifically the Hall parameter remain unchanged with an equal fractional change in both the magnetic field and in the pressure, it is expected that this process will become effective in stabilizing a 250 torr discharge with magnetic field strengths of only 0.4 T.

Pulsed discharge experiments were subsequently carried out; but as indicated in Chapter 2 the expected stabilization effect was not observable. In view of this fact, the initial assumptions about the scalability of this process became in doubt. As a consequence of this situation, the purpose of the investigation initiated and outlined in this chapter was to examine the time-domain evolution of the electron and ion drifts, in the hope of specifying a region of operation where these magnetic processes could indeed be successfully applied. Throughout the duration of this chapter the operating conditions are those specified in Table 3.1, and the design under consideration is the "Modified TEA Discharge System" shown in Figure 2.4.

3.1 Momentum Transfer Collisional Frequency

The momentum transfer collisional frequency represents the frequency in which a particle undergoes a change-of-momentum collision. This frequency is important in calculating the collisional effects upon the discharge, and hence the drift velocities of the gas particles. For electron-atom collisions, the collisional frequency is given by,[17]

$$\langle \nu_{m\text{-}e} \rangle \simeq N_n Q_{en(mix)} \left[\frac{8 k_b T_e}{\pi m_e} \right]^{1/2} . \qquad (3.1)$$

where N_n is the colliding species number density, and $Q_{en(mix)}$ is the collision cross section

Table 3.1 Fundamental Discharge Parameters.

Parameter	Value
Magnetic Field	0.41 T
Electric Field	6.7×10^5 V/m
Pressure	250 torr
Gas Mixture	1:1:8 $CO_2/N_2/He$
Gas Temperature	300 K

Table 3.2 Momentum Transfer Cross Sections.[18,19]

r - s	$Q_{rs}(10^{-20}\ m^2)^1$
e - He •	6.89
e - N_2 •	17.
e - CO_2 •	5.7
e - MIX •	7.78
He - MIX	18.7
N_2 - MIX	32.6
CO_2 - MIX	42.0
MIX - MIX	22.4

• valid for low energy (0.5 to 2.5 eV) electrons

MIX refers to the laser gas mixture

1. = 1:1:8 $CO_2/N_2/He$

for electrons colliding with neutral gas atoms. The average electron temperature, given by T_e, is determined with the aid of Figure 3.1, where the normalized distribution function for the electrons is theoretically calculated. With this figure, T_e is estimated as being the most probable value in the electron energy distribution function. Therefore with an E/N of 8×10^{-16} V/cm², T_e is ≃ 1.9 eV. Using this value for the electron temperature, and the cross sectional information given in Table 3.2, the collisional frequency in a 1:1:8 $CO_2/N_2/He$ gas mixture at 250 torr is:

$$\nu_{m\text{-}e} = 5.77 \times 10^{11}\ s^{-1}\ . \tag{3.2}$$

For atoms or molecules colliding with the neutral gas, the collisional frequency for momentum transfer becomes:[17]

$$\langle \nu_{m\text{-}n} \rangle = N_n Q_{n\text{-}mix} \left[\frac{16 k_b T_n}{\pi m_n} \right]^{1/2}\ . \tag{3.3}$$

where N_n, $Q_{n\text{-}mix}$, T_n, m_n, are the neutral gas density, collision cross section, temperature and mass of a single gas molecule. The expression for the two collision frequencies differs by a factor of square root 2. This additional factor arose in equation (3.3) because the ion and neutral gas temperatures were nearly the same value.

Again using the data for the various momentum transfer cross sections in Table 3.2, the collisional frequency for a 1:1:8 gas mixture at T_n = 300 K becomes:

$$\nu_{m\text{-}He} = 1.66 \times 10^{9}\ s^{-1} \text{ and} \tag{3.4}$$

$$\nu_{m\text{-}mix} = 1.99 \times 10^{9}\ s^{-1} \tag{3.5}$$

for the helium atoms, and gas mixture, respectively.

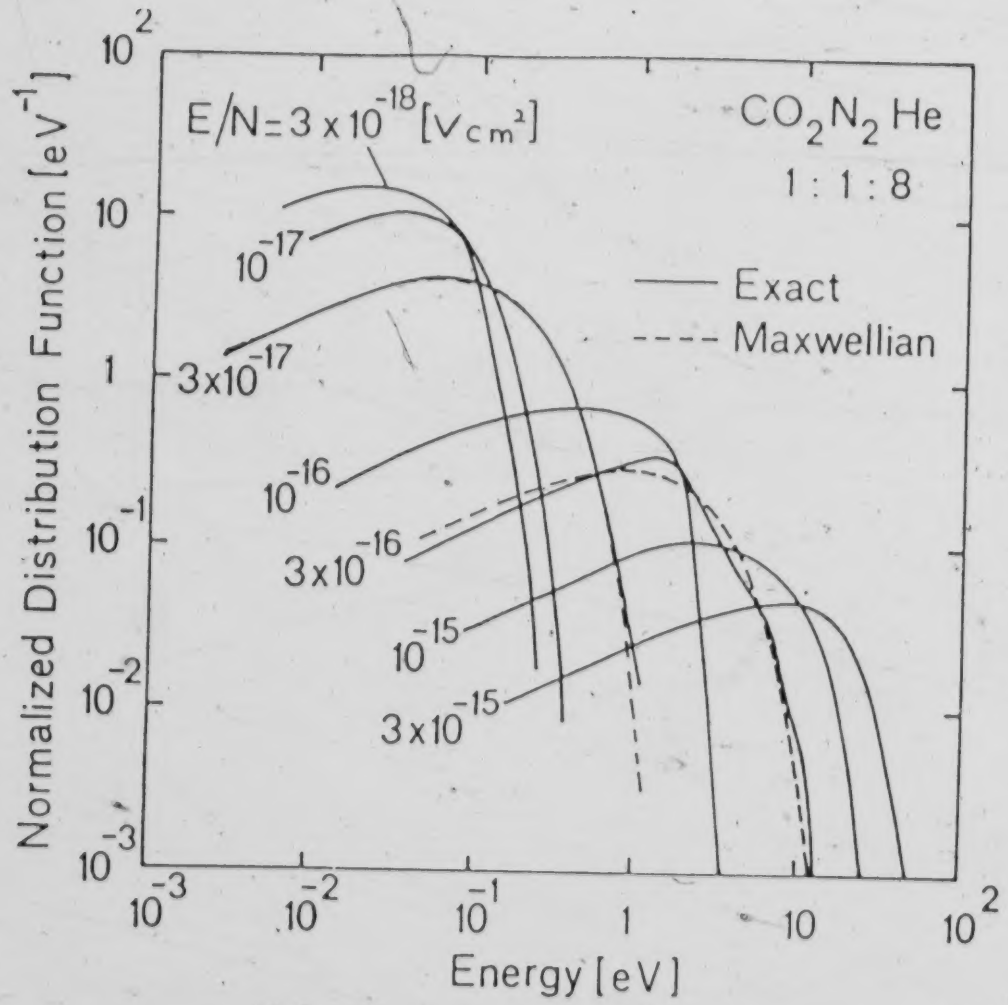

Fig. 3.1 Derived Distribution Functions of Electrons.[20]

3.2 Cyclotron Frequency

When a charged particle travels in a magnetic field, the Lorentz force causes the particle to gyrate in a helical orbit about that magnetic field line, provided that the particle is free to travel without collisions. The frequency that a particle gyrates about the magnetic field line is called the cyclotron frequency and is given by: [17]

$$\omega_{c\text{-}n} = \left[\frac{q_n B}{m_n}\right], \tag{3.6}$$

where n represents the particle undergoing the gyration. Without any scattering collisions the electrons and ions will continue to gyrate about this magnetic field line at the rates of:

$$\omega_{c\text{-}e} = 7.21 \times 10^{10}\ s^{-1}, \tag{3.7}$$

$$\omega_{c\text{-}He^+} = 9.88 \times 10^{6}\ s^{-1} \text{ and} \tag{3.8}$$

$$\omega_{c\text{-}mix} = 3.81 \times 10^{6}\ s^{-1} \tag{3.9}$$

respectively for electron, helium ion, and gas mixture ions. This frequency, in conjunction with the collisional frequency, is important in the determination of whether or not magnetic fields play an important role in particle motion. The parameter which utilizes these values is called the Hall parameter and is described in the following section.

3.3 Hall Parameter

As stated previously, the Hall parameter is useful in gauging the strength of the magnetic field, in relation to particle motion. Specifically the Hall parameter is defined as: [17]

$$\beta_n = \frac{\omega_{c\text{-}n}}{\nu_{m\text{-}n}}, \tag{3.10}$$

where n again refers to the particle in question. If both the cyclotron and the collisional frequency are of the same magnitude, then the Hall parameter reveals that the charge carriers will on average undergo one gyration about the magnetic field line before they suffer a momentum scattering collision. Therefore, the larger the Hall parameter, the more dominant is the role of the magnetic field.

Initially the motivation behind this project was to produce a Hall parameter as high as possible. In this way magnetic field effects would be increasingly important. Values of at least unity were sought for this purpose. Unfortunately in the actual experimental system developed for this project the maximum achievable Hall parameters were only

$$\beta_{e\text{-}mix} = 0.125 \text{ , and} \tag{3.11}$$

$$\beta_{He^+\text{-}mix} = 0.006 \text{ .} \tag{3.12}$$

It is obvious that with these low values for the Hall parameter the magnetic field strengths available could not be expected to play a significent role in discharge characteristics. A calculation of the Lorentz drift and an optimum Hall parameter, which provides a maximum drift velocity, is determined in the following section.

3.4 Drift Calculation

To calculate the drift velocity for the electrons and ions, a fluid model for each species is used with the assumption of a weakly ionized gas. This fluid model is given by the following momentum equation,[17]

$$mn\frac{\partial \mathbf{u}}{\partial t} + \frac{\partial}{\partial \mathbf{x}} P\hat{I} + mn\mathbf{u}\cdot\frac{\partial \mathbf{u}}{\partial \mathbf{x}} = nq(\mathbf{E} + \mathbf{u} \times \mathbf{B}) - mn\nu_m \mathbf{u} - m\mathbf{u}S \text{ ,} \tag{3.13}$$

where $\mathbf{u}$, and $\mathbf{x}$, are the velocity and position vectors while P and $\hat{I}$ are the pressure and unit tensor respectively and S is a source term.

The above equation can be simplified with the following assumptions,

$$\frac{\partial \mathbf{u}}{\partial t} \simeq 0 \text{ and,} \qquad S = 0 \text{ .}$$

The justification for these assumptions is as follows. For time scales larger than $1/\nu_m$, the first term in equation (3.13) is small and can be considered to be zero. Secondly the source term is zero, since a free electron source, such as an electron beam, is not used. Thus S can be assumed to be zero as well. In addition, since particle gradient drifts are small in a nearly

homogeneous electric discharge, the second and third terms in equation (3.13) can also be approximated to be zero. Therefore, using these conditions the momentum equation simplifies to the following form:

$$\mathbf{u} = \frac{nq(\mathbf{E} + \mathbf{u} \times \mathbf{B})}{mn\nu_m} . \tag{3.14}$$

Breaking this down into velocity components, assuming that the magnetic field is in the z-direction, and the electric field is in the negative y-direction, yields:

$$u_x = \frac{\omega_c^2 E}{B(\nu_m^2 + \omega_c^2)} , \text{ and} \tag{3.15}$$

$$u_y = \frac{\nu_m^2 \mu E}{\nu_m^2 + \omega_c^2} , \tag{3.16}$$

where μ is the mobility and equals $q/m\nu_{m\text{-}e}$ for the electrons. The velocity component in the x-direction is the **E** x **B** drift term, while the y-component of the velocity is the standard mobility dependent drift term.

For a better insight into the variables effective in modifying the magnetically induced drift velocity, u_x, this term can also be written in the following form:

$$u_x = \frac{\mu\beta E}{1 + \beta^2} , \tag{3.17}$$

where β is the Hall parameter.

As can be seen from equation (3.17), a maximum in the drift velocity, u_x, occurs when the Hall parameter equals unity. In the present system under study, the maximum drift velocity is reached at field strengths of 3.28 and 111 T, for the respective electron and helium ion cases. Table 3.3 provides the actual drift velocities calculated for this system, plus drift velocities at magnetic field strengths of 3.28 and 111 T. It is obvious from Table 3.3 that helium ions do not move significantly during the duration of a 300 to 1000 nanosecond discharge. In fact, on these these time scales, the typical distance for electron drift is only 2.5 cm for a 1 μs discharge. Although a 2.5 cm drift distance may seem large, by the time the electron has traversed the entire discharge length of 3 cm, its actual drift is only 3.7 mm. The

Table 3.3 Electron - Ion E x B, and E-Field Drift Velocities.

B in tesla	E-Field dir. u_y in m/s	E x B dir. u_x in m/s	Species
0.41	2.01×10^5	2.51×10^4	e^-
0.41	1.71×10^3	6.30	He^+
3.28	1.02×10^5	1.02×10^5	e^-
3.28	1.71×10^3	50.4	He^+
111.	179.	6.04×10^3	e^-
111.	854.	854.	He^+

$\mu_e = 0.305\ m^2/Vs$ $\mu_{He^+} = 2.55 \times 10^{-3} m^2/Vs$

2.5 cm drift is non-physical and would only occur if the electron were free to drift for a 1 μs duration. Since the electron traverses the interelectrode volume in 150 ns, the actual interelectrode drift is only 3.7 mm. Furthermore, instabilities originate on, or near the cathode surface in a region called the cathode fall. For a 1:1:8 gas mixture, at 250 torr, the cathode fall distance is only 45 μm in length. Thus the actual E x B drift experienced by each electron, as it traversed the cathode fall, was only 5.6 μm. As explained in Chapter 1, for magnetic stabilization to be effective, the electron E x B drift has to be sufficient to inhibit the formation of a thermal hot spot. Shown in Figure 3.2 is a schematic of this process. The mechanisms involved here are as follows. Initially a free electron is emitted from the cathode surface and drifts in both the E, and E x B field directions. After traveling some distance, the electron excites or ionizes a gas particle, as shown in step 1. When an ionization collision occurs, a positively charged ion is created. This ion then drifts in the -E field direction, as shown in step 2. The reason that the average ion drift in the E x B direction is negligible, is that its Hall parameter is so small. Thus magnetic field effects are minimal. The third step in the drift process occurs when the ion collides with the cathode. When this occurs, there is a chance that an electron will be emitted from the cathode. The transverse distance labeled "d" on Figure 3.2, is the distance between the initial electron and the emitted electron. This distance must be sufficient such that after a time smaller than the instability formation time, the cumulative distance d grows sufficiently large, that further secondary electron emission appears to be contained in a different "hot" channel. Since the "hot" channels, or instability scale lengths, are typically 1 mm in diameter, this process must be repeated several times to provide net drift distances of 1 mm.

To determine these times, new values for u_{ye}, u_{yion}, and u_{xe} must be calculated, since the electric fields within the cathode fall are different from those in the positive column. This situation arises since there is a fixed voltage drop, independent of pressure, across the cathode fall region. With a cathode fall voltage of 188 volts over a distance of 45 μm, the resulting electric field is $\simeq 4.15 \times 10^6$ V/m. Because of this relatively high electric field, the average electron temperature increases to about 20 eV. As a consequence of this condition, the new

Collisions Involved in the Drift Calculation

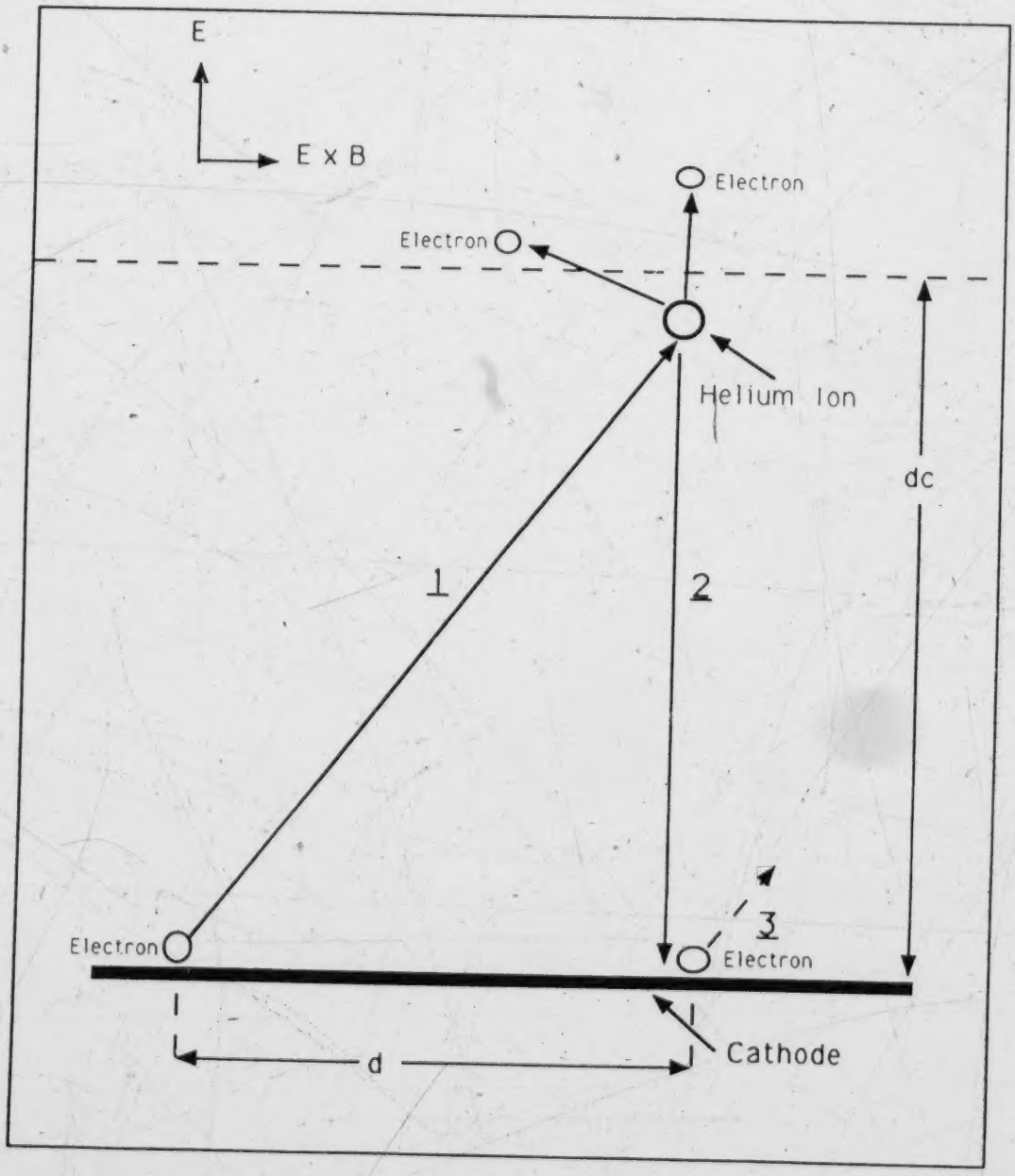

Fig. 3.2 Drift Trajectories and Distances.

electron and ion drift velocities become:

$$u_{ye} = 3.89 \times 10^5 \text{ m/s}, \qquad u_{yion} = 9.13 \times 10^3 \text{ m/s}$$

$$\text{and } u_{xe} = 1.50 \times 10^4 \text{ m/s}.$$

In calculating the net drift distance, as shown in Figure 3.2, it is assumed that all electron production is created at the end of the cathode fall region. Since electron production is in reality created throughout the entire cathode fall distance, the electron drift calculated below will be smaller then the actual distance; thereby giving a conservative estimate of that result. Thus the time necessary for the drift process to be completed, as outlined in Figure 3.2, is given by the sum of the electron and ion transit times through the cathode fall which occurs in 5.0 ns. Two hundred such occurrences are therefore possible in a 1.0 μs discharge. Consequently, the actual E x B drift distance experienced by the electrons becomes

$$\frac{dc \times u_{xe}}{u_{ye}} \times 200 = 347 \ \mu\text{m}. \tag{3.18}$$

Drift distances of $\simeq$ 0.4 mm are close to the instability scale length of $\simeq$ 1 mm. However, this calculation assumes that the discharge will be stable for the entire duration. Clearly if the stability of the discharge is such that instabilities arise in times less than 1.0 μs, then the actual drift distances will be correspondingly smaller. An investigation into probable instability mechanisms is presented in the next section, in order to provide some additional insight into this critical instability formation time.

3.5 Instability Mechanisms

Extensive theoretical and experimental work has documented that there are several instability mechanisms which can become manifest in gas lasers. The more common of these include, attachment-induced ionizational, and thermal instabilities, as well as streamer formation. The first mechanism, electron attachment or ionizational instability, results in the

creation of striations, or ionizational waves throughout the discharge volume. Although this process is essentially independent of pressure or electric power density, it is heavily dependent upon electron temperature. In the case of TEA discharges, the overvoltaged plasma is quite energetic. As a result, the electron temperature is sufficiently large that this instability mechanism is not of great significance. The second mechanism, thermal instabilities, results from localized gas heating and usually leads to plasma constriction. Heating of the plasma occurs whenever the power transferred into the vibrational mode of a molecule decays into translational degrees of freedom. In addition, this process is very dependent upon pressure, and electric power density. Consequently, the limit to the electric power density that a plasma can sustain can be determined from these considerations. The other instability mechanism, streamer formation, is of more importance in higher E/N discharges where large ionization coefficients produce large electron avalanches. Streamer formation, as shown in Figure 3.3, occurs when the pressure times a distance d, less than the interelectrode separation, becomes large enough to permit the space-charge field of a single avalanche head to become comparable to the applied electric field. This is satisfied when the Townsand first ionization coefficient, α, multiplied by the discharge distance, d, becomes greater than 20, and is referred to as the Raether breakdown criterion. When this occurs, subsidiary electrons, initiated by photoionization, will tend to converge toward the strong electric field region of the primary avalanche head. This results in creating a highly conducting filamentary channel, or spark, in times shorter than those possible by the mobility restricted electron transit times.

Since the magnetic stabilization concept is not applicable to the stabilization of an avalanche head, the thermal instability formation time will be the only mechanism for which a detailed description is presented.

3.6 Thermal Instability Formation Time

As indicated above, the formation time of a thermal instability is very dependent upon the neutral gas pressure, and the input electric power density. A criterion for this instability mechanism, in terms of a growth rate parameter, ν_g, has been formulated by Haas[21] as:

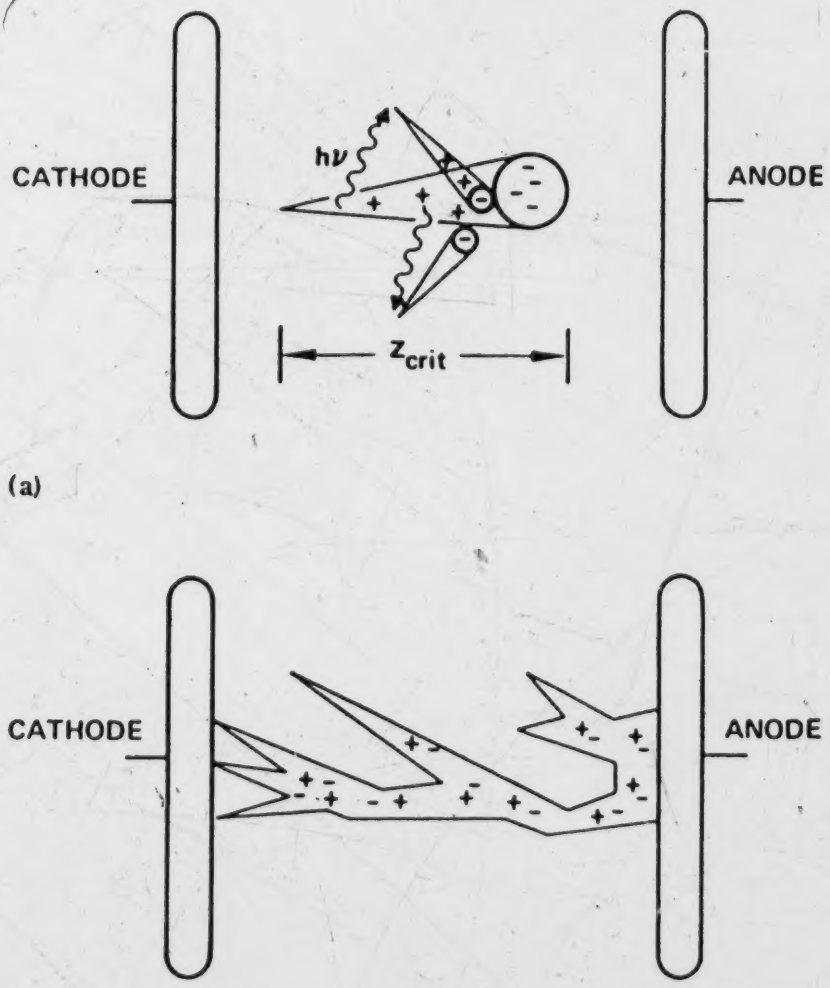

Fig. 3.3 Raether Breakdown in Pulsed Discharges.[22]

$$\nu_g = \frac{-b}{2} \pm \frac{1}{2}(b^2 - 4c)^{1/2} \text{ in } s^{-1} \text{ where,} \tag{3.19}$$

$$b \simeq \frac{1}{(nC_pT)}\left[\frac{\kappa_T T}{l^2} + \frac{nC_pT}{\tau_{VT}} + JEF_v(2 + \hat{\tau}_{VT}) + JEF_T\left[\frac{\delta n_e/n_e}{\delta n/n}\right]\right], \tag{3.20}$$

$$\text{and } c \simeq \frac{1}{nC_pT\tau_{VT}}\left[\frac{\kappa_T T}{l^2} + JE\left[\frac{\delta n_e/n_e}{\delta n/n}\right]\right]. \tag{3.21}$$

The variables used in this equation are defined in Table 3.4.

Nighan and Wiegand[24] have further advanced this formulation, as a function of electric power density, to model a CW CO_2 convection laser discharge. In the present laser excitation geometry, the gas ratios, power densities, and many other operational parameters are considerably different from those assumed by Nighan and Wiegand. In Figure 3.4 a plot of equation (3.19) is given for a 1:1:8 gas mixture at 250 torr. As can be seen from this figure, the plasma begins to go unstable in times less than 1 μs for input power densities of JE $\geq$ 100 KW/cm^3. In TEA laser discharges these power densities are usually exceeded and values near 1 MW/cm^3 are not uncommon. Specifically, in the "Modified TEA Laser Discharge System" of Figure 2.4, input power densities into the plasma were in the 300 - 700 KW/cm^3 range. At these power densities, thermal instabilities occur in 350 to 800 ns. As a consequence of this fact, high power TEA discharges have an inherent limitation with respect to the length of the excitation pulse. With this limitation in mind, the magnetic stabilization process becomes severely limited when applied to pulsed discharges. Thus for an instability formation time of 500 ns, one can extrapolate from the data to find a value of the magnetic field which will give drifts of 1 mm, which are sufficient to quench instability formation in such a discharge.

To calculate the required magnetic field strength, one must examine how the values of u_{yion}, u_{ye}, and u_{xe} change with an increase in magnetic field. Since $\beta_{He^+\text{-}mix}$ is relatively small for a reasonable increase in magnetic field strength, $\omega_{c\text{-}mix}$ should still be much less than the collisional frequency $\nu_{m\text{-}mix}$. As a consequence, u_{yion} is still collisionally dominated. Therefore, equation (3.16) is not altered by a modest increase in B. Hence u_{yion} is approximately constant. The opposite is true for u_{ye} and u_{xe}, since their Hall parameter,

Table 3.4 Variables used in Equation 3.19.[22]

Symbol	Name of Variable
n	Neutral Gas Density in m^{-3}
C_p	Specific Heat at Constant Pressure[23] in $\frac{J}{K}$
T	Temperature in K
κ_T	Thermal Conductivity[23] in $\frac{W}{m\,K}$
l	Instability Scale Length[24] in m
τ_{VT}	V-T Relaxation Time[25] in s
J	Current Density in $\frac{A}{m^2}$
E	Electric Field in $\frac{V}{m}$
F_V	Fractional Power Transfer into the Vibrational Mode[26]
F_T	F. P. T. into the Translational Mode[26]
$\hat{\tau}_{VT}$	$\frac{\partial \ln(\tau_{VT})}{\partial \ln(T)}$ ref. 25
$\left[\frac{\delta n_e / n_e}{\delta n / n}\right]$	$\frac{-2\hat{k}_i \sin^2\phi + \hat{\nu}_{u'}}{2\hat{k}_i \cos^2\phi + \hat{\nu}_{u'}}$ at $\phi = 90°$
$\hat{k}_i$	$\frac{\partial \ln(k_i)}{\partial \ln(T)}$ ref. 27
$\hat{\nu}_{u'}$	$1 + \hat{\nu}_u - \hat{\nu}_m \cos(2\phi)$[28,29]

THERMAL INSTABILITY GROWTH TIME

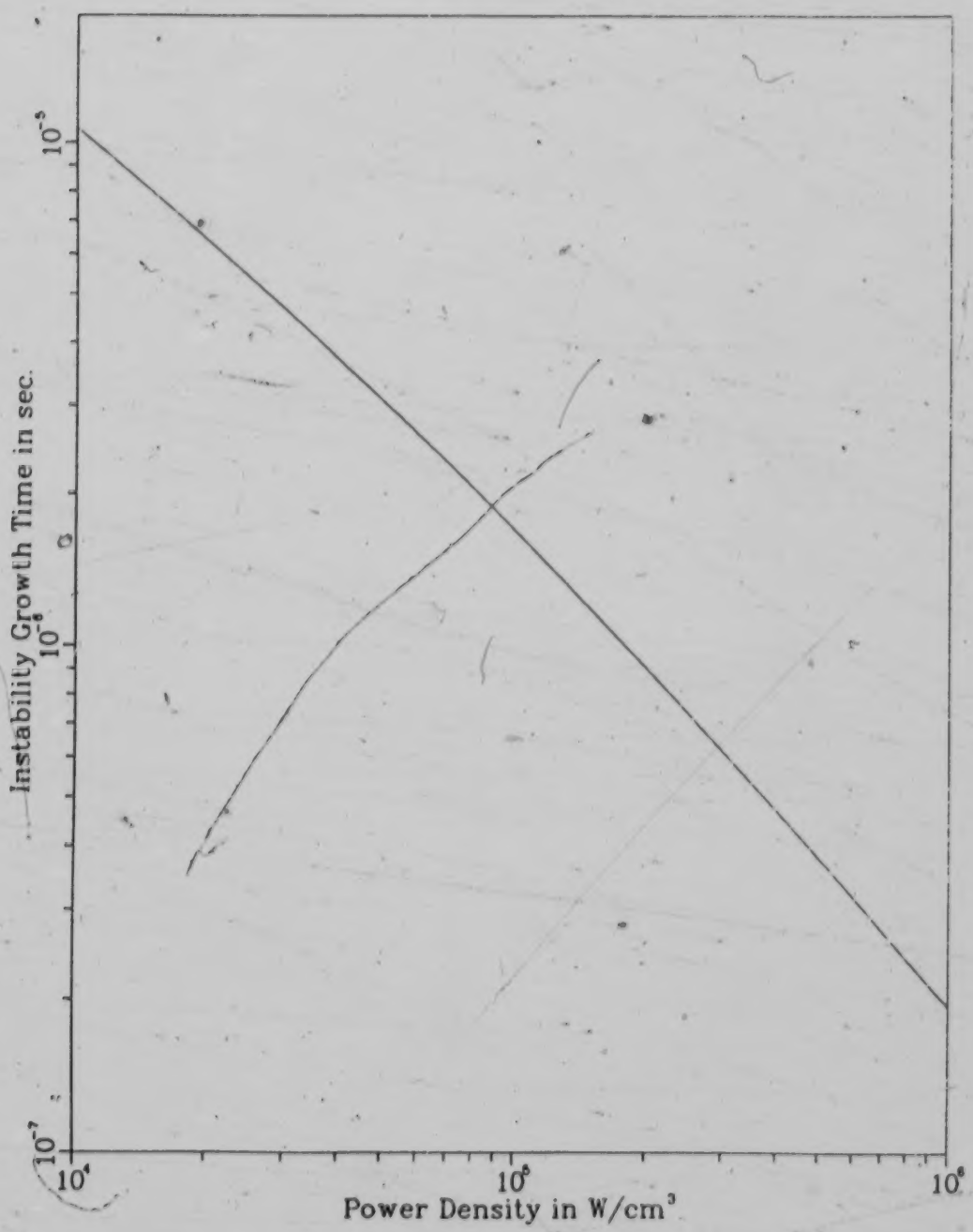

Fig. 3.4 Thermal Instability Formation Time.

$\beta_{e\text{-}mix}$, is closer to unity. At the operating conditions of $E = 4.15 \times 10^4$ V/m and $\mu_{ion} = 2.2 \times 10^{-3}$ m²/V s, eqn (3.16) reveals that $u_{ion} = 9.13 \times 10^3$ m/s. This implies that the ion transit time through the 45 μm cathode fall occurs in approximately 5 ns, this provides the electron with 100 sequential periodic trips. With this in mind, each electron must drift 10 μm in order to collectively create a net drift of 1 mm. Thus with a single electron drift of 10 μm, equation (3.18) becomes

$$\frac{d_c \times u_{xe}}{u_{ye}} = 10\ \mu m \qquad \text{or} \tag{3.22}$$

$$\frac{u_{xe}}{u_{ye}} = \frac{2}{9} . \tag{3.23}$$

Upon substitution for u_{xe}, and u_{ye}, from equations (3.15) and (3.16), and with some simplification we obtain:

$$B = \frac{2\, m_e\, \nu_{m\text{-}e}}{9\, q} . \tag{3.24}$$

In the cathode fall region, $\nu_{m\text{-}e} = 1.87 \times 10^{12}\ s^{-1}$. Thus for single electron drifts of 10 μm, the required magnetic field strength is 2.37 T. In other words, with magnetic fields of $\simeq$ 2.4 T, electron drifts of near 1 mm occur for discharges of 500 ns duration. Since these field strengths were not attainable with the apparatus previously developed for the project, effective magnetic stabilization of pulsed discharges unfortunately became beyond the reach of this present investigation. In the following chapter, the experimental data gathered in support of this fact will be presented.

4. RESULTS

In Chapter 3 it was shown theoretically that to achieve magnetic stabilization of pulsed discharges at pressures near 250 torr would require magnetic field strengths in the 2.4 T range. Since field strengths of such a magnitude were not attainable with the available test apparatus, only the much lower fields near 0.4 T were used, in an attempt to obtain some measure of verification that magnetic stabilization could indeed be effectively utilized in pulsed discharges. Justification for this experiment arose from the fact that the instability scale length of ≈ 1 mm, was determined from the literature as a best approximation to the actual scale length. At 0.41 T, induced electron drifts are ≈ 0.3 mm. Thus if the 1 mm estimate is larger than the actual instability scale length, then some effect might still be observable. With this premise in mind, this chapter discusses the experimental results obtained with the "Modified TEA Discharge System", shown in Figure 2.4, along with the theoretical calculations for drift distance and discharge stability.

4.1 Experimental Discharge Data

Several experiments were performed in order to determine if any effect in the discharge could be seen with the application of magnetic fields, or the abscence of those fields. Tables 4.1 to 4.3 give the relevant data derived from these experiments. In Table 4.1, data for excitation pulses of 300 ns duration are presented. As can be seen, stable discharges were obtainable at gas pressures from 125 to 400 torr over large variations in the applied potential. Since instabilities were not present during these short excitation times, the low E x B drift distance of 0.13 mm was not utilized for discharge stabilization. By further increasing the excitation length it was hoped that the discharge would become unstable. The data for pulse lengths of 800 ns duration are given in Table 4.2. Again, the discharge was observed to be stable at pressures from 250 to 500 torr, both with and without a magnetic field. As a consequence, when the magnetic field was applied across the discharge, the

0.33 mm E x B drift was again not utilized in discharge stabilization. Since the 12:14:74 $CO_2/N_2/He$ gas mixture was found to be inherently stable under the above conditions, any magnetic stabilization effect could not be ascertained. Consequently two additional features were added to the experiment. These procedures were to progressively increase the excitation length and/or the input power density into the discharge volume until such time as instabilities could be observed. Thus upon application of the magnetic field, any discharge stabilization effect could be observed. This procedure, although not difficult, was not as convenient as changing the gas mixture to create a border-line stable plasma. With such a plasma, discharge stability experiments identical to the one explained above were done. In Table 4.3 experimental data obtained for various gas mixtures are presented. A border-line stable plasma was created with a 23:27:50 gas mixture, at a 15 KV applied potential. To determine if magnetic fields could indeed stabilize this discharge, applied magnetic fields of 0.28 T were induced transverse to the discharge. The results of such an experiment are displayed in Table 4.4. As can be seen from this table, there were 6 stable discharges in a sample of 10 sequential runs, without any magnetic field. However, when a 0.28 T field was applied there were only 4 stable discharges. Therefore, with only 10 discharge runs for each case, we see that the magnetic field did not stabilize the discharge. These findings were consistent with Chapter 3, since the E x B drift distance experienced in this experiment was only $\simeq$ 0.3 mm; which is considerably shorter than the estimated minimum value of 1 mm necessary for the process to become effective.

Further studies with the plasma V-I characteristics were done. Figure 4.1 shows the V-I characteristics of a 12:14:74 $CO_2/N_2/He$ mixture at gas pressures from 250 to 500 torr, and with magnetic fields from 0 to 0.41 T. The purpose of this study was to determine if magnetic fields could maintain a stable discharge, even though power densities were sufficient to make a non-magnetic field plasma unstable. As can be seen from this figure the V-I characteristics were nearly identical between the magnetic and non-magnetic cases. Unfortunately, problems with the behavior of the experimental system prevented the accumulation of experimental points higher up on the V-I curve. Without those additional points it could not be conclusively determined whether or not magnetic fields would produce a

Table 4.1 Data on a 12/14/74 Mixture with a 300 ns Excitation Length

P in torr	V in KV	I in KA	Result	Drift in mm
125	12 → 25	1.8 → 4.8	stable	0.13
250	12 → 21	1.0 → 3.2	stable	0.13
400	15 → 27	0.8 → 3.4	stable	0.12

Table 4.2 Data on a 12/14/74 Mixture with a 800 ns Excitation Length

P in torr	V in KV	I in KA	Result	Drift in mm
250	15 → 24	2.4 → 5.8	stable	0.34
400	15 → 24	1.3 → 4.4.	stable	0.33
500	20 → 24	2.0 → 3.4	stable	0.33

Table 4.3 Data on a Variable $CO_2/N_2/He$ Mixture with a 1 μs Excitation Length

P in torr	Mix. Ratio	V in KV	Result
50	1.0/0.0/0.0	21	arc
100	0.0/1.0/0.0	18	arc
250	36/32/32	15 → 20	arc
250	13/13/74	15	stable
260	23/27/50	15	transition
500	12/14/74	15 → 23	arc

Table 4.4 Magnetic Field Effects On a Border-line Unstable Plasma

Discharge Result 0.0 T	Discharge Result 0.28 T
stable	arc
arc	stable
stable	stable
stable	arc
stable	stable
arc	stable
arc	arc
arc	arc
stable	arc
stable	arc

23:27:50 $CO_2/N_2/He$ Discharge at 260 torr, with a 800 ns excitation duration. Drift distances were 0.31 mm.

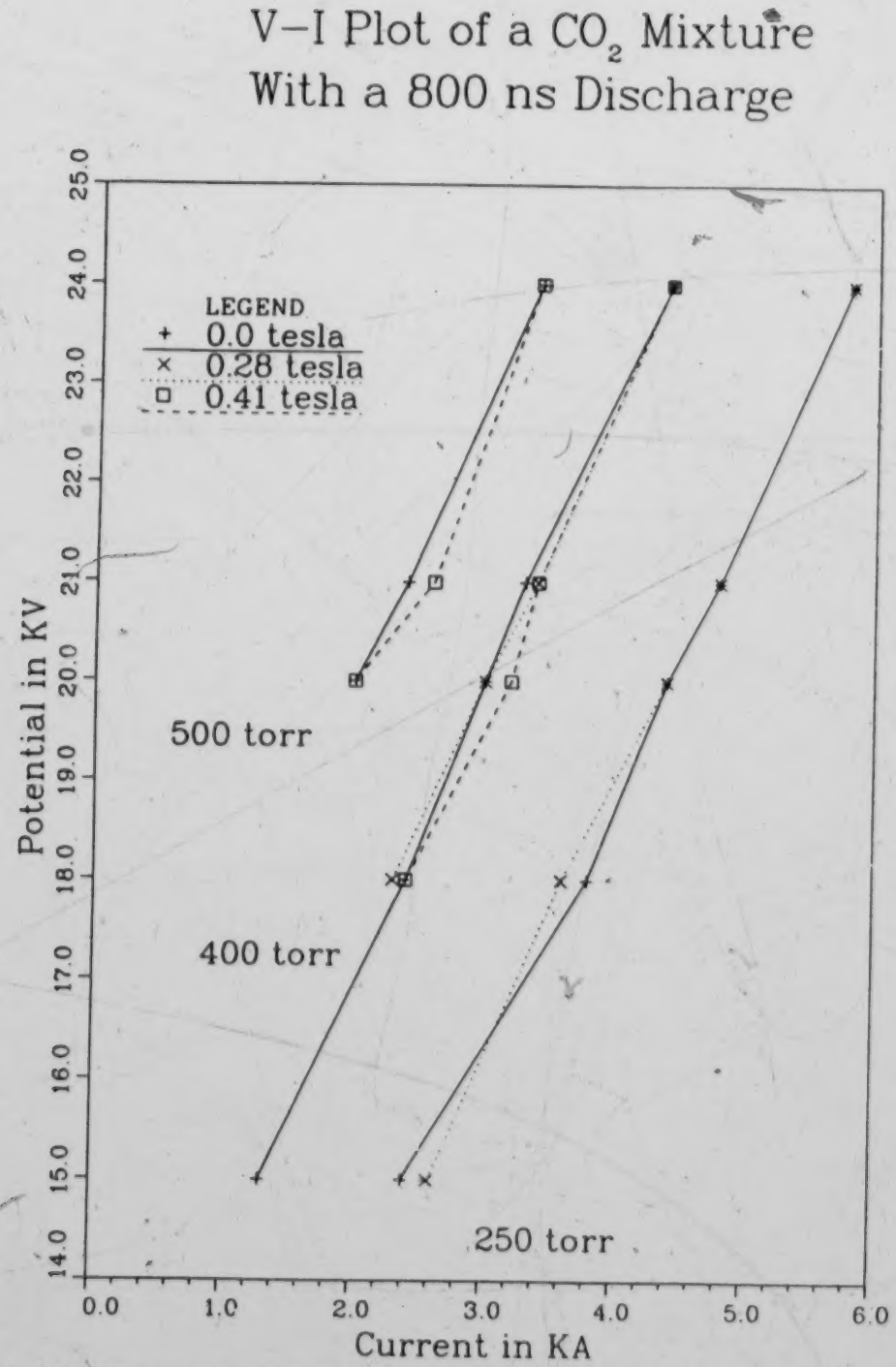

Fig. 4.1 V-I Characteristics of a 12:14:74 $CO_2/N_2/He$ Mixture from 250-500 torr, with Magnetic Fields from 0 to 0.41 T.

higher power loading in the plasma.

In Chapter 3, a theoretical analysis concluded that when a plasma begins to go unstable, stabilization can only become effective if E x B drift distances equal or exceed 1 mm, within the instability formation time. Moreover, since calculations indicated that 2.4 T magnetic fields are necessary for the stabilization of a 500 ns discharge, further increases in the power loading into the plasma would clearly not result in a stable discharge. Any effective use of magnetic stabilization, once it becomes effective, would be to keep the power loading in the plasma constant and increase the excitation duration. Therefore, for a practical extension of the magnetic stabilization process in pulsed discharges one would not look for extremely high power loadings, but rather moderate power loadings for indeterminately long excitation durations.

5. CONCLUSIONS

The theoretical and experimental results presented in this thesis have shown the difficulties involved in the application of magnetic stabilization to TEA discharges. Although the magnetic field strengths experimentally available were insufficient to observe the transition region between stable and unstable discharges, it was still possible to theoretically calculate the fields necessary to observe this stabilization transition. The analysis revealed that a transition will occur when magnetic fields are near 2.4 T in magnitude and are applied transverse to the electric field direction.

In the design of a test vessel for magnetic stabilization experiments, several problems had to be overcome. These problems included creating a low inductance circuit, necessary for high power pulsed excitation, and achieving magnetic fields of at least 0.4 T. The first problem was solved with the use of a cylindrical discharge geometry in which the magnet was separate from the discharge circuit. The other problem of generating the 0.4 T magnetic field was eventually overcome utilizing a vane geometry electromagnet. The initially projected value of 0.4 T required to achieve stabilization was based upon an extrapolation of the magnetic stabilization results in a low pressure CW laser discharge.

In this system, operating at 30 torr gas pressure, magnetic fields of 0.04 T were predicted as sufficient to observe the stabilization effect. Because electron drift velocity is dependant upon the Hall parameter,

$$\beta_e = \frac{\omega_{c\text{-}e}}{\nu_{m\text{-}e}} \qquad \text{which is proportional to } \frac{B}{N},$$

at 250 torr gas pressure, the calculated value of 0.4 T should have exhibited a stabilizing influence.

In Chapter 3, an explanation of why these 0.4 T magnetic fields were ultimately found to be insufficient for the task at hand revealed that a further parameter needed to be

considered. This parameter was the instability formation time. At the power densities required for high pressure excitation, this instability formation time is on the order of several hundred nanoseconds, thereby restricting the excitation duration to this same time interval. This limitation, apparently inherent in pulsed operation, differs from the CW magnetically stabilized case in the following way. Low pressure thermal instability onset occurs on a millisecond time scale. However, for an order of magnitude increase in gas pressure, and at the power densities required for TEA discharges, this thermal instability onset period reduces by over three orders of magnitude. Since the magnetic E x B drift has only a few hundred nanoseconds to stabilize the discharge, the interval during which this process can operate is not linearly scalable, as previously expected. Thus, in order to achieve stabilization in a TEA discharge at 250 torr, the magnetic fields must be increased by at a factor of 60.

Once the difficulties involved with the scalability of this process have been overcome, the application of magnetic stabilization in TEA discharges will still differ from its CW excitation counterpart. Specifically, in CW laser systems magnetic stabilization has enabled a higher power loading of the plasma to be achieved. However, the application of this process to TEA discharges is not expected to be useful in maintaining a higher power loading. Rather, the process would be beneficial when long excitation durations are required for the reason that once the plasma begins to be stable through the use of magnetic fields, the stability of the plasma is independent of excitation duration, thereby accomplishing the initial goal of this thesis.

Because of the recent development of third generation permanent magnet materials having unusually high cohesive forces, an alternative source of intense magnetic fields has recently become available. This new generation of magnets, made with the rare earth Samarium, can produce permanent magnetic fields in the 2 - 3 T range. One manufacturer of such magnets is Sherritt Gordon Ltd., located in Fort Saskatchewan Alberta Canada. With the use of these Samarium magnets, the inefficient electromagnet now becomes obsolete since the radially profiled magnetic field can be created with a non dissipative permanent magnet structure. With such a discharge system, verification of the magnetically stabilized pulsed

discharge should be attainable.

REFERENCES

[1] Seguin V. A., *A MAGPIE Coaxial CO_2 Laser System*, Ph.D. Thesis, University of Alberta, Canada (1986)

[2] Razdan R., *Magnetic Stabilization of Laser Gas Discharges*, Ph.D. Thesis, University of Alberta, Canada (1987)

[3] Willis R., *Axial Laser Discharge Stabilization With Rotating Magnetic Fields*, Ph.D. Thesis, University of Alberta, Canada (1987)

[4] Antoniuk D., *A Magnetohydrodynamic Approach to Laser Discharge Stabilization*, Ph.D. Thesis, University of Alberta, Canada (1983)

[5] Maiman, T. H., *Stimulated Optical Radiation in Ruby Masers*, Nature, **187**, 493 (1960)

[6] Johnson L. F., Nassau K., *Infrared Fluorescence and Stimulated Emission of Nd^{3+} in $CaWO_4$*, Proc. IRE, **49** 1702 (1961)

[7] Geusic J. E., Marcos H. M., Van Uitert L. G., *Laser Oscillations in Nd-doped Yttrium Aluminum, Yttrium Galluim and Gadolimuim Garnets*, Appl. Phys. Lett., **4** 182 (1964)

[8] Snitzer E., *Optical Maser Action of Nd^{3+} in a Barium Crown Glass*, Phys. Rev. Lett., 7 444 (1961)

[9] Patel C. K. N., *Interpretation of CO_2 Optical Maser Experiments*, Phys. Rev. Lett., **12** 588 (1964)

[10] Dumanchin R., Rocca-Serra J., *Augmentation de l'energie et de la puissance fournie par unite de volumn dans un laser a CO_2 en regime*, C.R. Acad. Sci., **269**, 916 (1969)

[11] Beaulieu A. J., *Transversely Excited Atmoshperic Pressure CO_2 Lasers*, Appl. Phys. Lett., **16**, 504 (1970)

[12] Cherrington B. E., *Gaseous Electronics And Gas Lasers*, Pergamon, Oxford (1979)

[13] Rhodes C., *Excimer Lasers*, Springer-Verlag, New York (1984)

[14] The measurement of the pulsed magnetic field was done by measuring the induced emf, ϵ, on a wire loop.

[15] The formula which was used is $B(max) = \frac{\epsilon\tau}{8A}$ where τ is the period of oscillation of the induced emf and A is the area of the loop.

[16] This formula gives values which are 21% lower than the actual field since the area under a cosine curve was approximated to be a triangle.

[17] Sutton G. W., Sherman A., *Engineering Magnetohydrodynamics*, McGraw-Hill, Toronto (1965)

[18] Elliot C. J., Judd O. P., Lockett A. M., Rockwood S. D., *Electron Transport Coefficients and Vibrational Excitation Rates for Electrically Excited CO_2 Lasers*, Los Alamos Scientific Laboratory Research Report LA-5562-MS (1974).

[19] The collisional cross sections for ions and neutrals were calculated using $Q_{r\text{-}s} = \pi(r_r + r_s)^2 = Q_{s\text{-}r}$, where the radii for He, N_2, and CO_2 are 11, 18.9, and 23.3 nm respectively.

[20] Witteman W. J., *The CO_2 Laser*, Springer-Verlag, New York (1987)

[21] Haas R., *Plasma Stability of Electric Discharges in Molecular Gases*, Phys. Rev. A **8**, 1017 (1973)

[22] Palmer A., *A Physical Model on the Initiation of Atmospheric-Pressure Glow Discharges*, Appl. Phys. Lett., **25** 138 (1974)

[23] Weast R., *CRC Handbook of Chemistry and Physics 64TH Edition*, CRC Press, Boca Raton Florida (1983)

[24] Nighan W., Wiegand W., *Causes of Arcing in C.W. CO_2 Convection Laser Discharges*, Appl. Phys. Lett., **25** 633 (1974)

[25] Taylor R., Bitterman S., *Survey of Vibrational Relaxation Data for Processes Important in the CO_2-N_2 Laser System*, Rev. Mod. Phys. **41** 26 (1969)

[26] Nighan W., *Electron Energy Distributions and Collision Rates in Electrically Excited N_2, CO, and CO_2*, Phys. Rev. A, **2** 1989 (1970)

[27] Wiegand W., Nighan W., *Plasma Chemistry of CO_2-N_2-He Discharges*, Appl. Phys. Lett., **22**, 583 (1973)

[28] Hake R., Phelps A., *Momentum-Transfer and Inelastic-Collision Cross Sections for Electrons in O_2, CO, and CO_2*, Phys. Rev., **158** 70 (1967)

[29] Engelhardt A., Phelps A., Risk C., *Determination of Momentum Transfer and Inelastic*

Collision Cross Sections for Electrons in Nitrogen Using Transport Coefficients, Phys. Rev., 135 A1566 (1964)